



**HAL**  
open science

# Characterization of the vertical size distribution, composition and chemical properties of dissolved organic matter in the (ultra)oligotrophic Pacific Ocean through a multi-detection approach

P. Fourier, Gabriel Dulaquais, C. Guigue, P. Giamarchi, G. Sarthou, H. Whitby, R. Riso

## ► To cite this version:

P. Fourier, Gabriel Dulaquais, C. Guigue, P. Giamarchi, G. Sarthou, et al.. Characterization of the vertical size distribution, composition and chemical properties of dissolved organic matter in the (ultra)oligotrophic Pacific Ocean through a multi-detection approach. *Marine Chemistry*, 2022, 240, pp.104068. 10.1016/j.marchem.2021.104068 . hal-03544177

**HAL Id: hal-03544177**

**<https://cnrs.hal.science/hal-03544177>**

Submitted on 31 Oct 2023

**HAL** is a multi-disciplinary open access archive for the deposit and dissemination of scientific research documents, whether they are published or not. The documents may come from teaching and research institutions in France or abroad, or from public or private research centers.

L'archive ouverte pluridisciplinaire **HAL**, est destinée au dépôt et à la diffusion de documents scientifiques de niveau recherche, publiés ou non, émanant des établissements d'enseignement et de recherche français ou étrangers, des laboratoires publics ou privés.

1 **Characterization of the vertical size distribution, composition and chemical**  
2 **properties of dissolved organic matter in the (ultra)oligotrophic Pacific**  
3 **Ocean through a multi-detection approach**

4  
5 **P. Fourrier<sup>1</sup>, G. Dulaquais<sup>\*1</sup>, C. Guigue<sup>2</sup>, P. Giamarchi<sup>3</sup>, G. Sarthou<sup>1</sup>, H. Whitby<sup>4</sup> & R.**  
6 **Riso<sup>1</sup>**

7  
8 <sup>1</sup>Laboratoire des Sciences de l'Environnement Marin CNRS UMR 6539, Institut Universitaire Européen de la  
9 Mer, Université de Bretagne Occidentale. Place Nicolas Copernic - 29280 Plouzané, France, <sup>2</sup>Aix-Marseille  
10 Univ., Université de Toulon, CNRS, IRD, MIO UM 110, Marseille, France, <sup>3</sup>Laboratoire OPTIMAG, Université  
11 de Brest, 6 Av. Victor Le Gorgeu, 29285, Brest Cedex, France, <sup>4</sup>Department of Earth, Ocean and Ecological  
12 Sciences, School of Environmental Sciences, University of Liverpool, Liverpool, UK.

13  
14 \*Corresponding author. Email: gabriel.dulaquais@univ-brest.fr.

15  
16 **Abstract**

17 This work presents a multi-analytical approach for the characterization of marine dissolved  
18 organic matter (DOM). The determination of marine dissolved organic carbon (DOC) was  
19 performed by size exclusion chromatography (SEC) and validated using a certified reference  
20 material (CRM) as well as through an intercomparison exercise. Multi-detection SEC,  
21 fluorescence and electrochemical methods were used in order to describe the size distribution  
22 spectra, the composition and chemical properties of marine DOM, in the (ultra)oligotrophic  
23 West Tropical South Pacific Ocean (WTSP). In this work, we defined the state of degradation  
24 of DOC in the different size fractions, operationally defined by SEC. We estimated that on  
25 average 62% of DOC was of humic nature (0.5 – 10 kDa), of which ~ 9% was able to  
26 complex trace elements, such as iron (Fe). Our results tend to support that non-refractory  
27 DOC is of high molecular weight (HMW), nitrogen (N)-rich, aliphatic, and has a weak  
28 fluorescence quantum yield and an enhanced binding capacity for Fe. The ageing of marine  
29 DOM occurring within mesopelagic waters is mainly driven by microbial respiration and  
30 alters these chemical properties. Although our results are in agreement with a paradigm  
31 describing oceanic DOM biogeochemistry known as the size-reactivity continuum, 3 µmolC  
32 L<sup>-1</sup> of very HMW (> 10 kDa) were still observed in a water mass mainly composed of Pacific  
33 Deep Waters. This persistence could be explained by a significant content (5%) of aromatic  
34 carbon that may protect HMW DOM from long term biodegradation.

35  
36 **Keywords:** Dissolved Organic Matter (DOM), Pacific Ocean, Humic Substances (HS), Size  
37 Exclusion Chromatography (SEC).

## 39 **1. Introduction**

40 Marine dissolved organic matter (DOM) is a large pool of reduced carbon (Mackenzie et al.,  
41 1981), representing an inventory of similar magnitude to atmospheric carbon. DOM is a  
42 complex mixture of thousands of compounds (Gu et al., 1995; Stedmond et al., 2003), mainly  
43 small molecules, with an extraordinary diversity of composition (Zark et al., 2017), that  
44 results from both abiotic and biotic processes occurring throughout the ocean interior (Hansell  
45 et al., 2009).

46 The size-reactivity continuum provides a paradigm for describing the oceanic  
47 biogeochemistry of DOM (Amon & Benner, 1996; Benner & Amon, 2015). According to this  
48 model, the ageing of highly (microbially) bioavailable freshly produced matter of high  
49 molecular weight (HMW) induce the production of small, oxidized, nitrogen-depleted  
50 compounds that are refractory to heterotrophic respiration. This process is thought to be the  
51 main pathway of recalcitrant DOM production, also called the microbial carbon pump (Hach  
52 et al., 2020; Jiao et al., 2010). The origin of the recalcitrance of DOM is still debated with on  
53 the one hand the dilution hypothesis (Arrieta et al., 2015) and on the other hand the molecular  
54 hypothesis (Shen & Benner, 2018) but can also result from a combination of both. The recent  
55 work of Shen & Benner (2020) tends to validate the fact that the molecular properties of  
56 DOM are the primary control on its microbial utilization in the ocean, highlighting the need to  
57 develop quantitative proxies of the chemical properties of DOM.

58 Quantification of DOM can be assessed by the determination of dissolved organic carbon  
59 (DOC) concentrations in order to identify the dominant process affecting the entire DOM pool  
60 (production vs. degradation) in the global ocean (Hansell et al., 2009). Nevertheless, the DOC  
61 concentration does not provide information on the nature of DOM and even less on its  
62 composition, therefore oceanic studies often combine DOC distributions to specific (structural  
63 characterization, Figure S1) or semi-specific qualitative analyses (inferred classification,  
64 Figure S1). Mass spectrometry and nuclear magnetic resonance (NMR) techniques are  
65 powerful tools to identify molecular formulae and chemical functions in DOM (Benner, 2003;  
66 Hertkorn et al., 2013; Kujawinski, 2011; Kujawinski et al., 2009; Mopper et al., 2007; Ogawa  
67 & Tanoue 2003 Osterholz et al., 2021). However, these methods need a solid phase extraction  
68 (SPE) step prior to analysis and due to the partial extraction yields of the SPE cartridge. At  
69 least a third of bulk DOM is lost during this extraction procedure (Dittmar et al., 2008).  
70 Moreover, due to the large seawater volume required, these techniques are not easily

71 applicable for oceanographic expeditions with restricted water budget, involving a large  
72 number of parameters. Therefore it is necessary to operationally classify organic compounds  
73 according to optical or chemical properties to study DOM biogeochemistry in the ocean.  
74 Optical properties of DOM help to identify biogeochemical processes occurring along the  
75 water column, and are used as proxies to study the quality (Coble, 2007; Fichot & Benner,  
76 2011), to trace the origin (Fellman et al., 2010; Osburn et al., 2016), and also as indicators of  
77 the biological and (photo)chemical processing (Del Vecchio & Blough, 2002; Helms et al.,  
78 2013; Osburn et al., 2016) of DOM. However, optical measurements by themselves do not  
79 provide robust information on the composition of DOM and need to be combined with  
80 complementary analyses. This is supported by a recent critical review of fluorescent DOM  
81 revealing the ubiquitousness of fluorescence spectra that « are not tied to biogeochemical  
82 origin, but exist across a wide range of different environments » (Wünsch et al., 2019). Semi-  
83 specific methods and size exclusion chromatography (SEC) are alternative approaches  
84 making it possible to easily differentiate the classes of DOM according to their size and  
85 polarity (Amy & Her, 2004; Bagtho et al., 2008; Cornelissen et al., 2008; Dittmar & Kattner  
86 2003; Dulaquais et al., 2018b; Huber & Frimmel, 1994; Huber et al., 2011). No sample  
87 extraction or purification are necessary prior to measurements. Coupled with various detectors  
88 (carbon, UV, nitrogen), this type of analysis represents an alternative method to study the  
89 biogeochemistry of DOM at large scales (Figure S1).

90 Progress in SEC combined with multiple-detection approaches has made it possible to  
91 operationally separate size fractions of DOM, to quantify their DOC content and to describe  
92 some of the chemical properties (Amy & Her, 2004, Dulaquais et al., 2018b, Huber et al.,  
93 2011). Among others, biopolymers (BP) correspond to a fraction of HMW (> 10 kDa)  
94 believed to be mostly constituted of extracellular polymeric substances, such as  
95 polysaccharides, proteinaceous material and amino sugars. SEC further permits an operational  
96 definition of humic substances (HS) of molecular weight ranging between 0.5 and 10 kDa  
97 based on their retention time (e.g. chemical affinity) on a polymethacrylate gel (Huber et al.,  
98 2011). Aquatic HS were historically divided into humic acids, which precipitate at  $\text{pH} \leq 1$ ,  
99 and fulvic acids soluble at any pH. With SEC, the HS fraction encompasses humic and fulvic  
100 acids. According to the literature, HS are believed to derive from phospholipids (Kowalenko  
101 & McKercher 1971; Stott & Martin 1990) or produced during the photooxidation of  
102 triglycerides and fatty acids (Kieber et al., 1997), but the chemical structure of HS varies  
103 depending on their origin (Ertel et al., 1984; Dulaquais et al. 2018a). Recent experiments also

104 proposed the dimerization of the amino acid tyrosine catalyzed by peroxidase as a possible  
105 pathway for HS production (Paerl et al., 2020). Carboxylic-rich alicyclic molecules (CRAM)  
106 may represent another significant fraction of operationally defined HS (Hedges et al., 1992).  
107 CRAM result from the decomposition of biomolecules derived from phytoplankton, exposed  
108 to microbial degradation in the ocean interior (Hertkorn et al., 2006) and could be important  
109 iron-binding ligands (Bundy et al., 2015). Part of the HS pool could also be formed during  
110 condensation reactions by intermolecular collisions of compounds derived from the  
111 degradation of BP (Lehmann and Kleber, 2015; Ogawa & Tanoue, 2003). These  
112 condensations occur according to Maillard reactions, between carbohydrates and amino acids  
113 or proteins, to form melanoidins (Maillard, 1912). SEC also operationally defines fractions of  
114 LMW such as building blocks (BB, 0.3 – 0.5 kDa), LMW acids (< 0.3 kDa, Huber et al.,  
115 2011), and LMW neutrals. These LMW fractions are thought to be derived from the fractions  
116 in the upper size range (Huber et al., 2011) in agreement with the size reactivity continuum.  
117 The BB fraction is supposed to correspond to degraded HS of LMW (Huber et al., 2011), the  
118 other two fractions contain, among others, mono-protonic organic acids, mono-  
119 oligosaccharides, alcohols, aldehydes, ketones and amino sugars (Amon & Benner, 1994;  
120 Huber et al., 2011).

121 Among the different chemical properties of DOM, the binding capacity for dissolved iron  
122 (dFe) is of particular interest. Indeed, it is a key element for marine life and DOM is well-  
123 known to enhance dFe solubility by organic complexation (Powell & Donat, 2001; Rue &  
124 Bruland, 1995, 1997; van den Berg, 1995; Wu & Luther III, 1995). Several dFe chelators  
125 have already been identified including siderophores, exopolysaccharides and humic-like  
126 ligands (Gledhill & Buck, 2012). Due to their relative refractory nature, humic-like ligands  
127 can be found in the deep ocean (Dulaquais et al., 2018a; Whitby et al., 2020a) and can thereby  
128 play an important role in the biogeochemistry of iron (Fe). Electrochemical methods are used  
129 to measure the concentrations of the electroactive humic-like substances in marine  
130 environments, which are thought to be the fraction of humic-like matter able to complex trace  
131 elements, such as Fe (eHS; Dulaquais et al., 2018a, 2020; Sukekava et al., 2018; Whitby &  
132 van den Berg, 2015). The quantification of eHS can be a complementary tool to track changes  
133 in the binding properties of DOM during its processing, with broader implications for our  
134 understanding of the interactions between DOM and trace elements.

135 In this work we propose a comprehensive view of marine DOM using multiple semi-specific  
136 analytical approaches. We present the size fractionation, the aromatic carbon content of DOM  
137 and its C:N composition along the entire water column in the oligotrophic gyre of the WTSP.  
138 It is commonly assumed that allochthonous DOM is higher in size and more aromatic than that  
139 of autochthonous origin. Aromaticity of DOM is one of the main indicators of sources and  
140 processes which influence DOM composition (Chen & Hur, 2015; McKnight et al., 2001).  
141 C:N elemental ratio of DOM is needed to determine its lability and the state of  
142 remineralization of its compounds. N-depleted DOM has been recognized as a typical feature  
143 of oligotrophic areas (Kähler & Koeve, 2001), and is further investigated in this manuscript.  
144 Samples were collected during the GEOTRACES TONGA (shallow hydroThermal sOurces  
145 of trace elemeNts: potential impacts on biological productivity and the bioloGicAl carbon  
146 pump, GEOTRACES GPpr14) and US-GP15 expeditions. We also studied the fluorescence  
147 properties of DOM and the electroactivity of humic-like substances. The latter analysis  
148 provided an estimation of the binding capacity of this humic carbon for dFe.

## 149 **2. Material and Methods**

### 150 **2.1 Sampling**

151 Samples were collected during two cruises (Figure 1a): TONGA (20° 24.431'S, 166°  
152 35.675'W, GEOTRACES GPpr14 onboard the R/V *L'Atalante* in November 2019) and  
153 GEOTRACES US-GP15 (leg 2, 19° 59.99'S, 152° 00.01'W, onboard the R/V *Roger Revelle*  
154 in November 2018). During the TONGA cruise, sampling was carried out using a trace metal  
155 clean polyurethane powder-coated aluminum frame rosette (TMR) equipped with twenty-four  
156 12 L Teflon-lined GO-FLO bottles (General Oceanics) and attached to a Kevlar® wire.  
157 Potential temperature ( $\theta$ ), salinity ( $S$ ), and dissolved oxygen ( $O_2$ ), were retrieved from the  
158 conductivity–temperature–depth (CTD) sensors (SBE9+) deployed on the TMR. The cleaning  
159 protocols of all the sampling equipment followed the guidelines of the GEOTRACES  
160 Cookbook (<http://www.geotraces.org>). After recovery, the TMR was directly transferred into  
161 a clean container equipped with a class 100 laminar flow hood. Samples were then taken from  
162 the filtrate of particulate samples (collected on acid cleaned polyethersulfone filters, 0.45  $\mu$ m  
163 supor) and collected into acid cleaned and sample-rinsed HDPE 125 mL bottles. Immediately  
164 after collection, samples were double bagged and stored at -20°C until analysis in a  
165 shorebased laboratory. Samples from the GEOTRACES US-GP15 expedition were collected  
166 using the Oceanographic Data Facility's (ODF, Scripps Institution of Oceanography) CTD  
167 rosette equipped with twelve 30 L Niskin bottles. Samples were filtered through 0.8/0.45  $\mu$ m

168 Acropak 500 filter cartridges and were stored in a -15°C freezer on board. Samples were  
169 returned frozen to Stanford University and stored at -20°C thereafter. Aliquots were  
170 subsampled in acid cleaned and ultrapure water rinsed 30 mL HDPE bottles at Stanford  
171 University within a laminar flow hood (class 100) and sent to LEMAR (Plouzané, France) in  
172 a cooler with ice packs (travel duration of 2 days) and finally stored at -20°C until analysis.  $\theta$ ,  
173 S, and O<sub>2</sub>, were retrieved from the CTD sensors (SBE9+) calibrated with onboard salinity and  
174 dissolved oxygen measurements by the ODF group. Details on CTD data access from the  
175 TONGA and US-GP15 expeditions are provided in the acknowledgments section.

## 176 2.2 Reagents

177 All aqueous solutions and cleaning procedures used ultrapure water (resistivity > 18.2  
178 MΩ.cm, MilliQ Element, Millipore®). The mobile phase for SEC multi-detection was a  
179 phosphate buffer (pH 6.85), prepared by dissolving disodium phosphate (Na<sub>2</sub>HPO<sub>4</sub>, 6 g,  
180 EMSURE®, 99.5%) and monopotassium phosphate (KH<sub>2</sub>PO<sub>4</sub>, 10 g, EMSURE®, > 99.5%) in  
181 ultrapure water (4 L). The acid phase was prepared by adding orthophosphoric acid (H<sub>3</sub>PO<sub>4</sub>,  
182 16 mL, EMSURE®, 85%) to a solution of potassium persulfate (K<sub>2</sub>S<sub>2</sub>O<sub>8</sub>, 2 g, Alfa Aesar,  
183 Ward Hill MA, USA, 97%) in ultrapure water (4 L). Calibrations of the organic carbon  
184 detector (OCD) and the ultra-violet detector (UVD) were achieved by potassium hydrogen  
185 phthalate (C<sub>8</sub>H<sub>5</sub>KO<sub>4</sub>, Alfa Aesar, 99.95 – 100.05%). The organic nitrogen detector (OND)  
186 calibration was done using urea standard solutions (CH<sub>4</sub>N<sub>2</sub>O, Merck, Germany, >99.5%).  
187 Calibrations were made in artificial seawater. The artificial seawater was prepared by  
188 dissolving sodium chloride (NaCl, 6.563 g, ChemaLab NV, Belgium, 99.8%), potassium  
189 chloride (KCl, 0.185 g, Merck, Germany, 99.999%), calcium chloride (CaCl<sub>2</sub>, 0.245 g,  
190 Prolabo, France, > 99.5%), magnesium chloride (MgCl<sub>2</sub>, 1.520 g, Merck, Germany, 99-  
191 101%), magnesium sulfate (MgSO<sub>4</sub>, 1.006 g, Sigma-Aldrich, USA, ≥99%), sodium  
192 bicarbonate (NaHCO<sub>3</sub>, 0.057 g, ChemaLab NV, Belgium, >99.7 %) in ultrapure water (250  
193 mL). Artificial seawater was then UV irradiated for 2 hours in order to remove all traces of  
194 organic contaminants. Fulvic (SRFA, 1S101F) and humic acids (SRHA, 1S101H) from the  
195 *Suwannee River* used to calibrate the molecular weights (MW) of the HS fraction were  
196 provided by the International Humic Substances Society (IHSS). The average molar masses  
197 for these fulvic (711 Da) and humic acids (1066 Da) were previously defined by Aiken et al.  
198 (1989). Deep seawater reference (DSR) samples were used to validate the DOC  
199 measurements and were provided by the *Hansell* research laboratory (batch 19, lot #03-19).  
200 Calibration solutions for Total Carbon Analyser (TOC-V) were prepared using C<sub>8</sub>H<sub>5</sub>KO<sub>4</sub> in  
201 ultrapure water. A solution of 4 µg L<sup>-1</sup> quinine sulfate dihydrate (QS, Acros Organics, VWR

202 Chemical, USA, >99%) in 0.1 M sulfuric acid ( $\text{H}_2\text{SO}_4$ , Fluka®, Sigma-Aldrich, Switzerland,  
203 >95%) was used for standardization of fluorescence units. For electrochemical analysis, an  
204 acidic solution (hydrochloric acid,  $\text{HCl}$ , 0.01 M, Suprapur®, >99%) of  $1.24 \mu\text{mol L}^{-1}$  iron  
205 (III) was prepared from a stock solution ( $1 \text{ g L}^{-1}$ , VWR, Prolabo, France). The borate buffer  
206 ( $\text{H}_3\text{BO}_3$ , 1M, Suprapur®, Merck, Germany, 99.8%) was prepared in 0.4 M ammonium  
207 solution ( $\text{NH}_4\text{OH}$ , Ultrapure normatom, VWR Chemical, USA, 20-22%). The potassium  
208 bromate solution ( $\text{BrKO}_3$ , 0.3 M, VWR Chemical, USA,  $\geq 99.8\%$ ) was prepared in ultrapure  
209 water. The SRFA (2S101F) standard stock solution ( $38.2 \text{ mg L}^{-1}$ ) was prepared in ultrapure  
210 water and was then saturated with Fe and equilibrated overnight before use. Exact  
211 concentration was determined by SEC analysis.

## 212 **2.3 Analysis of marine DOM**

### 213 **2.3.1 Size exclusion chromatography (SEC)**

214 The distributions of the different organic compound classes were performed by SEC coupled  
215 with an OCD, an OND and a UVD (DOC-Labor®, Karlsruhe, Germany) as previously  
216 described by Huber et al. (2011) for natural waters, and adapted for marine waters by  
217 Dulaquais et al. (2018b). Repeated analysis of DSR samples ( $\text{DOC}_{\text{DSR}} = 43.2 \pm 1.7 \mu\text{mol L}^{-1}$ ;  
218  $n = 5$ ; consensus value of lot #10-18:  $43 - 45 \mu\text{mol L}^{-1}$ ) ensures an accurate determination of  
219 DOC. The same method and configuration were applied for our samples, but with injection  
220 volumes of 2.5 mL. This sample volume was selected to decrease the limits of detection  
221 (LOD, Table S1) and to avoid the condensation of DOM observed for injection volumes  
222 greater than 3 mL (Dulaquais et al., 2018b). Two chromatographic columns ( $250 \text{ mm} \times 20$   
223  $\text{ mm}$ , TSK HW-50S, 3000 theoretical plates, Toso, Japan) allows the separation of DOM into  
224 five fractions of organic compounds with an optimal resolution (Baghoth et al., 2008). These  
225 fractions were described in order of retention as BP ( $> 10 \text{ kDa}$ ), HS ( $0.5 - 10 \text{ kDa}$ ), BB ( $0.3 -$   
226  $0.5 \text{ kDa}$ ), LMW monoprotic acids and neutrals ( $< 0.3 \text{ kDa}$ , Huber et al., 2011). Their  
227 respective hypothetical composition are described in detail in Huber et al. (2011), Dulaquais  
228 et al. (2018b) and in Table S1. In this study, C:N ratios were determined in two operationally  
229 defined fractions (BP and HS) and the OND was calibrated using urea (instead of nitrate)  
230 standards in order to take into account the oxidation yield of organic nitrogen into nitrate. The  
231 percentage of aromatic carbon ( $\%C_{\text{arom}}$ ) in an operationally defined given fraction was  
232 determined according to Riso et al. (2021). It is defined as the spectral absorption coefficient  
233 (SAC in  $\text{m}^{-1}$ ) at 254 nm divided by the organic carbon concentration (OC, in  $\text{gC m}^{-3}$ ) of the  
234 fraction, and then multiplied by a coefficient of 4.403 (in  $\%C_{\text{arom}} \text{ gC m}^{-2}$ ). This coefficient was



235 determined by the correlation between the %C<sub>arom</sub> and SAC to [OC] ratio from NMR data  
236 determined for a suite of IHSS standards (Riso et al., 2021).

### 237 **2.3.1 TOC-V analysis**

238 During the TONGA expedition, samples for DOC analysis by TOC-V were taken from a  
239 classical rosette equipped with twenty-four 12 L Niskin bottles. The samples were filtered  
240 under low vacuum (< 50 mm Hg) through 25 mm glass fiber filters (porosity ~ 0.7 µm, GF/F  
241 Whatmann) and transferred into 10 mL glass ampoules. The filtrates were then acidified with  
242 20 µL of H<sub>2</sub>SO<sub>4</sub> (95%-98%, Sigma Aldrich), then the ampoules were flame sealed and stored  
243 at 4°C until the analysis. DOC concentrations were measured in two replicates on a TOC-V  
244 (Shimadzu, Kyoto, Japan) according to Sohrin & Sempéré (2005). The method consist of high  
245 temperature (680 °C) platinum (Pt)-catalyzed oxidation coupled to non-dispersive infrared gas  
246 detection of carbon dioxide (CO<sub>2</sub>). Before injection, the samples were bubbled for 2 min with  
247 CO<sub>2</sub>-free air to purge inorganic carbon. The accuracy and system blank of the instrument were  
248 determined by the analysis of certified water references (batch 19, lot #03-19, *Hansell*  
249 Laboratory, Miami, Florida, USA). The nominal precision of the analysis procedure was  
250 within 2%.

### 251 **2.3.3 Fluorescence spectroscopy**

252 Fluorescence analyses were performed on samples from the TONGA expedition. Excitation  
253 emission fluorescence matrices (EEM) were generated using a spectrofluorometer Cary  
254 Eclipse (Agilent®) equipped with a 150 W xenon excitation lamp. Optical measurements  
255 were performed in a 1 cm quartz cell. For each measurement, excitation and emission  
256 bandwidths were fixed at 5 nm. EEM were recorded with λ<sub>Ex</sub> ranging from 200 to 450 nm  
257 with an interval of 5 nm between each spectrum, and λ<sub>Em</sub> ranging from 280 to 510 nm. The  
258 scanning speed was set at 1200 nm min<sup>-1</sup>. The nomenclature defined by Coble (1996)  
259 associates peaks B and T to proteinaceous tyrosine-like (λ<sub>Ex</sub> 225-275 nm, λ<sub>Em</sub> 300-320 nm)  
260 and tryptophan-like (λ<sub>Ex</sub> 225-275 nm, λ<sub>Em</sub> 320-380 nm) compounds respectively, and a peak  
261 M to marine humic-like substances (λ<sub>Ex</sub> 310-320 nm, λ<sub>Em</sub> 380-420 nm) (Coble, 1996; Hudson  
262 et al., 2007; Parlanti et al., 2000). To take into account the daily variations of the  
263 spectrofluorometer sensitivity, EEM were normalized to the water Raman signal area. A  
264 blank correction was carried out by subtracting the mean EEM from ultrapure water samples.  
265 Fluorescence signals of EEM were converted into quinine sulfate units (QSU; 1 QSU =  
266 fluorescence of 1 µg L<sup>-1</sup> of quinine sulfate in 0.1 M H<sub>2</sub>SO<sub>4</sub> at λ<sub>Ex</sub>/λ<sub>Em</sub> = 350/450 nm). This  
267 was performed in order to compare our fluorescent measurements with previous studies since  
268 QSU is a widely used fluorescence unit. The LOD were defined as three times the standard

269 deviation of fluorescence intensity for each fluorophore according to the nomenclature  
270 defined by Coble (1996), and were 0.9 QSU for peak B (tyrosine-like), 0.7 QSU for peak T  
271 (tryptophan-like) and 0.1 QSU for peak M (humic-like). In this work, we mostly focus on  
272 three fluorescence intensity indexes. The fluorescence index (FI,  $\lambda_{Ex}$  370 nm,  $\lambda_{Em}$  450/500  
273 nm; McKnight et al., 2001), the biological index (BIX,  $\lambda_{Ex}$  310 nm,  $\lambda_{Em}$  380/430 nm; Huguet  
274 et al., 2009) and the humification index (HIX,  $\lambda_{Ex}$  255 nm,  $\lambda_{Em}$  435-480/300-345 nm; Zsolnay  
275 et al., 1999) were calculated to trace the origin of marine DOM.

#### 276 **2.3.4 Analysis of electroactive humic-like substances (eHS)**

277 The determination of eHS was performed on samples from the TONGA expedition. Analyses  
278 were performed by cathodic stripping voltammetry (CSV) using a polarographic Metrohm  
279 663VA stand connected to a potentiostat/galvanostat (Autolab, Metrohm®) and to an  
280 interface (IME 663, Metrohm®). Data acquisition was done using the NOVA software  
281 (version 10.1). The method used in this study was initially developed by Laglera et al. (2007)  
282 and adapted by Sukekava et al. (2018). The method is based on the adsorption at pH 8 of an  
283 Fe-humic complex at the surface of a mercury drop electrode under oxidative potential (0 V  
284 vs Ag/AgCl) and its reduction during linear stripping of potentials (from 0 to -0.8 V vs  
285 Ag/AgCl). In the presence of 30 mmol L<sup>-1</sup> bromate, the reduction of the Fe-humic complex  
286 provides a quantitative peak at -0.5 V (vs Ag/AgCl) with an intensity proportional to the  
287 concentration. In this study, the pH of samples was set to 8.00 ± 0.05 by the addition of a  
288 borate buffer (final concentration 10 mM) and adjusted by small additions of an ammonia  
289 solution. All eHS initially present in a sample were Fe-saturated by the addition of 20 nmol L<sup>-1</sup>  
290 <sup>57</sup>Fe in order to determine the total eHS concentration. After equilibration, aliquots (15 mL) of  
291 the sample were placed into 3 different teflon® vials (Savillex®); among them two were  
292 spiked with a SRFA standard (2S101F; spiked of 50 and 100 µg L<sup>-1</sup>), and left for overnight  
293 equilibration. After equilibration, samples were placed into a Teflon® voltammetric cell and  
294 analyzed by linear sweep voltammetry after 180 s of nitrogen (N<sub>2</sub>) purge (Alphagaz®, Air  
295 liquide) and a 90 s deposition step. Since there is no certified reference material (CRM) of  
296 marine HS, all the results are provided in equivalent SRFA per liter. The use of SRFA for the  
297 determination of oceanic eHS may induce biais due to possible differences in composition  
298 between SRFA batches purchased and to the origin of this material. SRFA come from  
299 freshwaters with a high DOM load while the marine environment is characterized by low  
300 DOM concentrations. Furthermore freshwater and marine HS have different composition,  
301 including binding capacity for iron, as previously shown (Dulaquais et al., 2018a, Esteves et  
302 al., 2009; Riso et al., 2021). Efforts should be conducted to develop a program for the

303 production of a marine humic reference material. In absence of an oceanic reference material  
304 comparable to the DSR (for DOC) or SAFe (for dFe) samples, the use of this material permits  
305 the generation of intercomparable data between labs and studies. Actually this consensus  
306 material is easy to purchase and widely use by the scientific community (Bundy et al., 2015;  
307 Cabanes et al., 2020; Dulaquais et al., 2018a; Gao & Guéguen 2018; Laglera et al., 2019; Riso  
308 et al., 2021; Slagter et al., 2019; Sukekava et al., 2018; Whitby et al., 2020a,b). Errors were  
309 calculated based on statistical evaluation of a least squares linear fit to the data. The absence  
310 of quantitative signals in ultrapure water ensures no contamination all along the analytical  
311 process. Because no blank signal can be detected, the LOD was defined as three times the  
312 standard deviation of the lowest concentration measured ( $23.2 \pm 3.0 \mu\text{g eq-SRFA L}^{-1}$ ) and was  
313 estimated to be  $9 \mu\text{g eq-SRFA L}^{-1}$ .

314 The four different analyses applied to the respective cruises and stations are presented in  
315 Table S2.

### 316 **3. Results and discussion**

#### 317 **3.1 Hydrography**

318 The hydrography of the WTSP is described in detail by Fumenia et al. (2018), Wagener et al.  
319 (2018), Peters et al. (2018) and Villa-Alfageme et al. (2019). In this section we briefly  
320 describe the key features encountered. At the sampling locations, salinities ranged from 35.48  
321 to 36.15 and temperatures from 23.6 to 27.1°C in the upper 100 m. The oligotrophy of the  
322 domain was evidenced by the extremely low surface nutrient concentrations (Cutter et al.,  
323 2018; Guieu & Bonnet, 2019) and surface chlorophyll levels derived from satellite data  
324 (Figure 1a; MODIS-Aqua MODISA simulations; data from giovanni.gsfc.nasa.gov). At both  
325 stations our shallowest sampling depth (25 m) can be considered in the mixed layer and thus  
326 representative of surface waters. The thermocline was deep (100–600 m) and was sampled at  
327 several depths (Figure 1b). Along the thermocline, different watermasses were identified. The  
328 South Pacific Central Waters (SPCW) can be divided by their salinity into the Western  
329 (WSPCW) in the upper thermocline and the Eastern (ESPCW) component in the lower  
330 thermocline. Modified Equatorial Subsurface Waters (ESSW) may be identified between  
331 these two SPCW components. ESSW are known to be poorly oxygenated (Silva et al., 2009)  
332 and to have a similar density to SPCW (Sprintall & Tomczak, 1993; Wyrcki, 1967). Thereby  
333 the low oxygen concentrations observed in the middle of the thermocline (Figure 1b) were  
334 probably induced by an inclusion of ESSW in the SPCW. Below the thermocline, the  
335 intermediate waters (600–900 m) were mostly composed of a mix between Subantarctic Mode  
336 Waters (SAMW,  $26.80 \leq \sigma\theta \leq 27.06 \text{ kg m}^{-3}$ , Hartin et al., 2011) and Antarctic Intermediate

337 Waters (AAIW,  $27.06 \leq \sigma\theta \leq 27.40 \text{ kg m}^{-3}$ , Hartin et al., 2011). Due to the overlap of their  
338 potential density, an exact distinction between these two watermasses remains difficult thus  
339 they are often considered as a single watermass in the subtropical area (Fumenia et al., 2018).  
340 These two watermasses have distinct origins; SAMW are formed by the mix of Antarctic

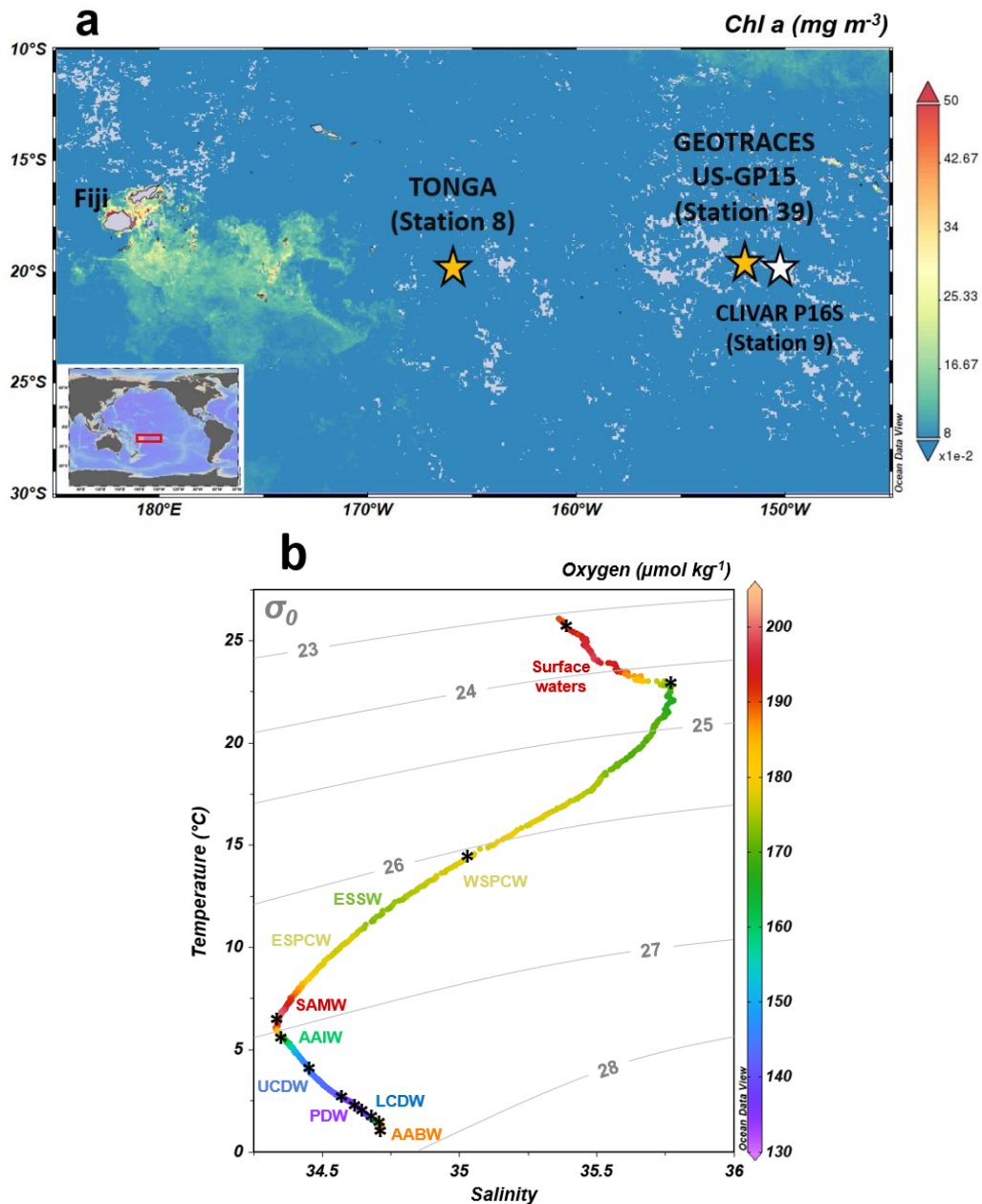


**Figure 1.** (a) Time averaged map of chlorophyll a ( $\text{mg m}^{-3}$ ; 8-daily 4-km over 2019-11-09 – 2019-12-09) in the Western Tropical South Pacific Ocean (WTSP). Figure generated using Giovanni ([giovanni.gsfc.nasa.gov](http://giovanni.gsfc.nasa.gov)). The two sampled sites of TONGA and GP-15 cruises are indicated (yellow stars), as well as the selected station from CLIVAR P16 for an intercomparison of dissolved organic carbon (DOC) concentrations (white star). (b) Temperature/salinity diagram of the study area with the color gradation corresponding to dissolved oxygen ( $\text{O}_2$ ) concentrations ( $\mu\text{mol kg}^{-1}$ ) at  $20^\circ 24.431'S$ ,  $166^\circ 35.675'W$  during the TONGA expedition. Grey lines indicate the isopycnal horizons (on the basis of potential density referenced to a pressure of 0 dbar). Water masses are indicated (see text for abbreviations). Asterisks (\*) indicate the samples collected for Size Exclusion Chromatography (SEC) analyses. Figure generated using ODV software.

341 surface waters with subtropical waters at the subantarctic zone, while AAIW originated from  
 342 deep convection of the densest Antarctic surface waters at the polar front zone. These distinct  
 343 locations of downwelling imprint the oxygen signature of these two watermasses, allowing us  
 344 to distinguish SAMW from AAIW by the higher oxygen content of SAMW ( $>200 \mu\text{mol kg}^{-1}$ ,

345 Figure 1b) according to McCartney (1979). In the deep sea (>1000 m) the two components  
346 (upper and lower) of the circumpolar deep waters (CDW) can be differentiated by their  
347 potential density ( $\sigma_{\theta_{UCDW}} = 27.59$ ,  $\sigma_{\theta_{LCDW}} = 27.79$ ; Peters et al., 2018; Figure 1b). CDW are  
348 the largest water masses of the Southern Ocean and are a mix of AAIW, North Atlantic Deep  
349 Waters (NADW) and intermediate water masses from the Pacific Ocean. CDW spread  
350 northward in the South Pacific from the Southern Ocean, alongside with the Deep Western  
351 Boundary Current (DWBC) of the Pacific Ocean, which flows along the western edge of the  
352 Southern basin (Koshlyakov & Tarakanov, 1999). UCDW and LCDW were separated by a  
353 layer, centered at 2900 m, mainly composed of PDW ( $\sigma_{\theta_{PDW}} = 27.77$ ; Peters et al., 2018;  
354 Figure 1b). This composite of PDW, UCDW and LCDW is transported northward at this  
355 location. In this work, this composite will be considered as the PDW. The most abyssal depths  
356 (> 4900 m) were occupied by a composite of LCDW and of Antarctic Bottom Waters  
357 (AABW), formed in the Ross Sea. These waters spread northward, driven by Ekman transport  
358 and forced by seafloor topography (Tomczak & Godfrey, 2003).

359

## 360 **3.2 Vertical distributions of fractions of dissolved organic marine compounds**

### 361 **3.2.1 DOC distribution**

362 The distribution profiles of DOC concentrations (Figure 2) of the four datasets showed a  
363 decrease from the surface to the deep waters. With the SEC method used for TONGA  
364 samples, the concentrations ranged from  $73.4 \pm 2.2 \mu\text{molC L}^{-1}$  at 25 m depth to  $37.4 \pm 1.1$   
365  $\mu\text{molC L}^{-1}$  in the old PDW composite at 3400 m, reflecting DOM mineralization in the  
366 mesopelagic zone. Deeper, DOC increased again to reach  $45.1 \pm 1.5 \mu\text{molC L}^{-1}$  at the deepest  
367 depth (5461 m). These concentrations were higher than the DOC signature of the AABW  
368 ( $40.2 \pm 0.7 \mu\text{molC L}^{-1}$  in the deep Southern Ocean, Bercovici & Hansell, 2016) located at  
369 these depths and could indicate benthic inputs of DOM by diffusion from sediments as  
370 previously proposed by Lahajnar et al. (2005) in the deep Atlantic Ocean. To validate DOC  
371 measurements, an intercomparison was performed between the DOC concentrations measured  
372 by our SEC-OCD system and data acquired using the « classical » TOC-V method. Results  
373 are presented in Figure 2 and the two datasets display similar vertical distribution and ranged  
374 of concentration for each depth interval. We further compared our measurements to the  
375 historic dataset from the P16 CLIVAR expedition at a station located at the same latitude but  
376 different longitude (20°S, 150°W) and it showed a good agreement between the three datasets  
377 in surface and deep waters. Scatter plot of the paired datasets shows that all the data were  
378 close to the 1:1 line (Figure S2) when uncertainties were considered. Good correlations of the

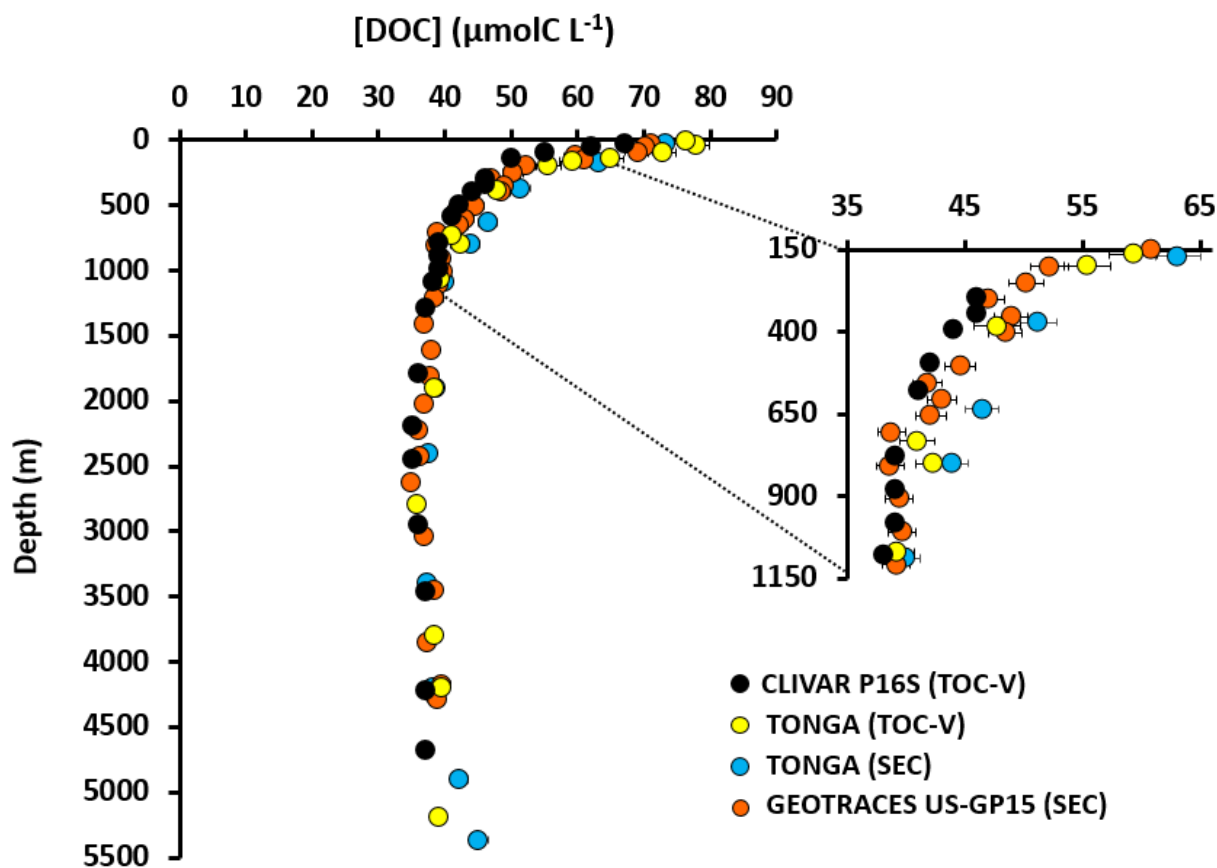


**Figure 2.** Intercomparison of the DOC concentrations ( $\mu\text{molC L}^{-1}$ ) of the TONGA expedition (GEOTRACES GPpr14) at  $20^{\circ} 24.431'S$ ,  $166^{\circ} 35.675'W$  measured by SEC (blue dots) and TOC-V (yellow dots). Data from the CLIVAR P16 cruise ( $20^{\circ}S$ ,  $150^{\circ}W$ ; Swan et al., 2009; dark dots) and from the GEOTRACES US-GP15 cruise ( $19^{\circ} 59.99'S$ ,  $152^{\circ} 00.01'W$ ) were also plotted (orange dots).

379 linear regressions ( $R^2 \geq 0.96$ ) and Spearman coefficients close to 1 (Figure S2), both indicate  
 380 the strong correlation between DOC concentrations determined by SEC and TOC-V. Together  
 381 with the accurate determination of DOC in DSR samples, this statistical demonstrate that the  
 382 SEC-OCD system has an excellent recovery of marine DOC and can be used for accurate  
 383 quantitative DOC assessment in an open ocean environment. Small discrepancies (see insert  
 384 Figure 2), higher than uncertainties of the methods, were observed in the mode waters and  
 385 could be explained by the hydrography. The  $\theta$ -S diagram shows only small differences in the  
 386 water composition between P16 and the two stations sampled (Figure S3a) with mode waters  
 387 being less haline at our locations than during the CLIVAR expedition. This difference of  
 388 intermediate water composition between  $\sim 400$  and  $\sim 700$  meters depth was however visible  
 389 by the higher apparent oxygen utilization (AOU) during both the CLIVAR and GP15  
 390 expeditions compared to TONGA (Figure S3b). The AOU represents the integrated oxygen  
 391 consumption by heterotrophic bacteria in the breakdown of organic matter and it is computed  
 392 as the difference between the oxygen saturation concentration, which depends on  
 393 thermohaline properties (Weiss, 1970) and the observed oxygen concentration. Thereby the

394 slightly higher DOC concentration we observed during TONGA (Figure 2) can be linked to a  
 395 lower DOC mineralization state at these depths than during CLIVAR P16. These observations  
 396 highlight the imprint of hydrography on DOC distribution.

### 397 3.2.2 Size class distribution and composition of DOM

398 The distribution of the different fractions composing DOM are presented in Figures 3a and in  
 399 Figure S4 (for TONGA and US-GP15 cruises, respectively). Along the water column, HS had  
 400 a quasi constant molecular weight ( $705 \pm 20$  Da) and was systematically the major fraction of  
 401 DOC ( $61.6 \pm 2.6$  %), with concentrations between 22.2 and  $43.2 \mu\text{molC L}^{-1}$ . LMW neutral  
 402 compounds represented the second most abundant fraction, contributing on average to 17.3%  
 403 of DOC, with an interval of concentration between 6.2 and  $11.2 \mu\text{molC L}^{-1}$ . The BB fraction  
 404 accounts for an average of  $9.7 \pm 1.3$  % of DOC throughout the water column, with  
 405 concentration varying between 3.3 and  $6.5 \mu\text{molC L}^{-1}$ . BP contributed to  $6.7 \pm 1.6$ % ( $2.0 - 8.0$   
 406  $\mu\text{molC L}^{-1}$ ) and the fraction containing LMW acids ( $1.1 - 4.5 \mu\text{molC L}^{-1}$ ) was the minor  
 407 component of DOC contributing to only  $\sim 4.7$ %.

408 Within all the different fractions, DOC concentrations decreased from surface to deep waters,  
 409 but small variations in the partitioning were however observed. For instance, the contribution  
 410 of the BP and of the LMW acids to DOC decreased from 25 m depth to the 2500-3000 m  
 411 depth and at the same time the contribution of LMW neutrals increased. These variations can  
 412 be interpreted as differences in the reactivity of the fractions. HMW compounds seem more  
 413 labile and consumed more rapidly than small neutral compounds that accumulate with ageing

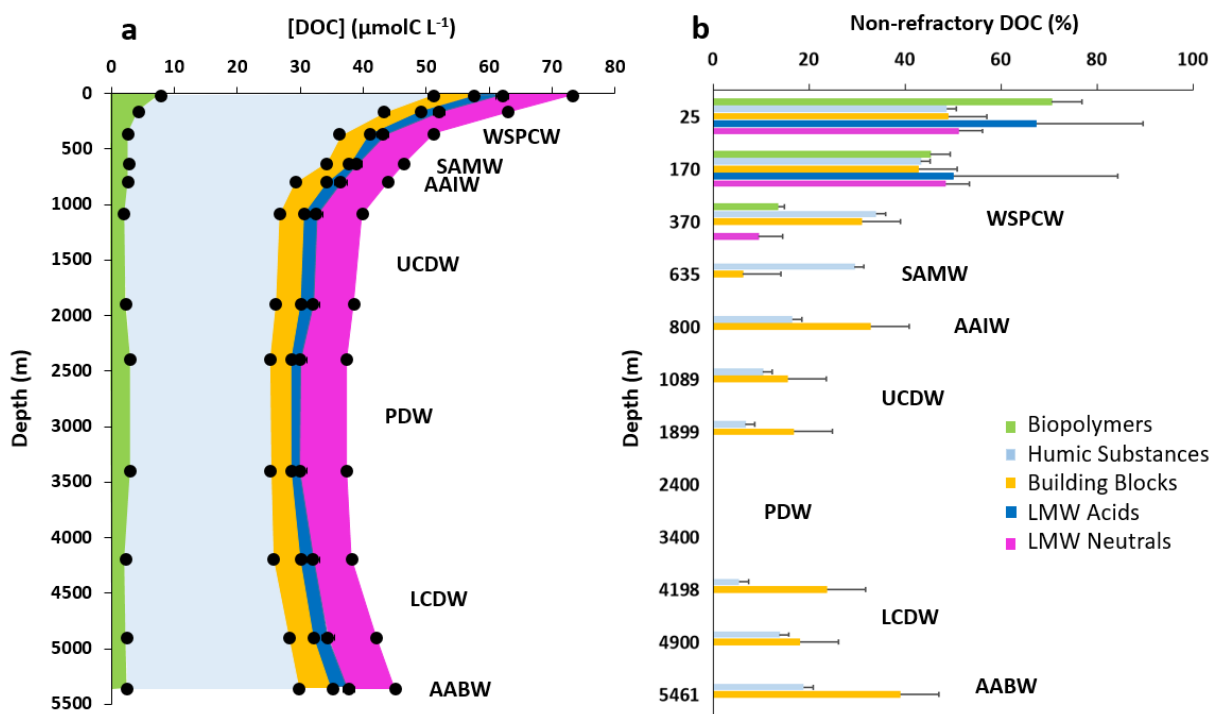


**Figure 3.** (a) Vertical profiles of the DOC concentrations ( $\mu\text{molC L}^{-1}$ ) in the five operational fractions defined by SEC. Non-visible error bars are covered by the symbols. (b) Percentage of non-refractory DOC calculated for each fraction (see text for explanation) as a function of depth (m). Depth of water masses are indicated (see text for abbreviations) at  $20^{\circ} 24.431'S$ ,  $166^{\circ} 35.675'W$  during the TONGA expedition (station 8).



414 of water masses. These observations are in agreement with the size reactivity continuum  
415 described by Benner & Amon (2015) and with the recent study of Zigah et al. (2017) that  
416 reports the size partitioning of DOC along the water column from surface to 3500 m depth in  
417 the oligotrophic North Pacific Ocean (Station ALOHA). Zigah et al. (2017) estimated a  
418 contribution of HMW DOC (defined in their study as > 1kDa) to be between 23 and 35%  
419 while LMW hydrophobic compounds (defined in their study as < 1kDa) retained by SPE  
420 cartridge accounted for 45-52% of DOC and LMW hydrophilic compounds (non-retained by  
421 SPE cartridge) were estimated to account for 22-33% of DOC. Similar to our observations,  
422 Zigah et al. (2017) measured HMW DOM throughout the water column and found humic-like  
423 substances (called LMW hydrophobic compounds in their study) to be the main fraction  
424 composing DOC. The authors further described a distribution of LMW hydrophilic  
425 compounds as quasi-homogeneous with a slight enrichment in the surface. The distribution  
426 they described is in excellent agreement with those we observed for both LMW acids and  
427 neutrals that are LMW hydrophilic compounds. In our study, seawater samples were analyzed  
428 without any pre-processing of samples. The excellent agreement of the size-distribution  
429 between our study and Zigah et al. (2017) shows that our method allows describing the size  
430 distribution of marine DOC with 2.5 mL of sample and without any preliminary filtration and  
431 extraction.

#### 432 *DOC refractivity within fractions*

433 At the latitude of sampling, the PDW has an age of over 1000 years (estimated using  
434 CLIVAR P16 inorganic  $\Delta^{14}\text{C}$  at 21°S and ageing equation proposed by Hawco et al., 2018). It  
435 has been shown that the organic  $\Delta^{14}\text{C}$  is even more depleted in the deep Pacific Ocean than  
436 the inorganic  $\Delta^{14}\text{C}$  (Zigah et al., 2017). Thereby DOC can be considered as almost only  
437 composed of refractory DOC (RDOC) in this watermass. Due to its refractory nature, the  
438 distribution of RDOC is assumed to be conservative (Ogawa & Tanoue, 2003) and can  
439 therefore be considered homogeneous throughout the water column. As a result, the DOC  
440 concentrations measured for each fraction in the PDW composite can be used to define the  
441 contribution of non-RDOC in the different fractions at each depth ( $[\text{non-RDOC}] = [\text{DOC}] -$   
442  $[\text{DOC}]_{\text{PDW}}$ ). Despite caveats implied by this assumption (e.g. possible photodegradation of  
443 RDOC in the upper euphotic zone, Polimene et al., 2018) it provides a working hypothesis to  
444 investigate the chemical properties and reactivity of semi-labile and refractory compounds.  
445 The contribution of non-RDOC for each fraction during the TONGA expedition was  
446 calculated for both stations throughout the water column (Figure 3b) and showed a decrease

447 from surface to the PDW composite depths (2400-3400 m). In surface waters more than 50%  
448 of DOC was non-refractory reaching up to 70% for the BP fractions. The decrease of non-  
449 RDOC with depth, down to the PDW composite, is observed for all fractions (Figure 3b) and  
450 is in agreement with the lability paradigm. However some differences among the fractions  
451 were observed with non-RDOC being undetectable in the LMW acids, LMW neutrals and BP  
452 fractions below 400 meters depth (Figure 3b) while non-refractory HS, and BB were still  
453 depicted. These differences in the non-RDOC distributions are representative of variabilities  
454 in the reactivity of the fractions and can be interpreted as the existence of semi-refractory  
455 compounds in the BB and HS fractions that were not measured in the other fractions.

456 *Aromatic carbon content of DOM*

457 The aromaticity of DOC was determined for all fractions except for the fraction of LMW  
458 neutrals wherein no quantifiable aromatic signal was detected (Figure 4a). In the oligotrophic  
459 WTSP, DOM was poorly aromatic with the percentage of aromatic carbon always below 5%  
460 in all fractions. In agreement with Medeiros et al. (2015) and Osterholz et al. (2021), our  
461 measurements showed surface samples of the Pacific Ocean with extremely low aromatic  
462 carbon content and the percentage of aromatic carbon increasing with depth in the upper 1000  
463 m. The higher percentages were observed for the BP and BB fractions in the PDW (2500 –  
464 3500 m). The maximum of aromaticity of BP and BB (~ 5%) is close to those observed for  
465 SPE-DOM in the Atlantic Ocean (grey area Figure 4a, 4.57 – 5.13 %C<sub>arom</sub>; Hertkorn et al.,  
466 2013) suggesting that the BP and BB are partly representative of the compounds retained on a  
467 SPE cartridge. According to the size-reactivity continuum, occurrence of BP should be  
468 limited in old water-masses. However, recent findings suggest that, among others, dissolved  
469 black carbon is likely an important fraction of refractory DOM (RDOM) in the ocean  
470 (Benner, 2003; Coppola & Druffel, 2016; Dittmar & Koch, 2006; Dittmar & Paeng, 2009;  
471 Nakane et al., 2017; Ziolkowski & Druffel, 2010). Black carbon are compounds with

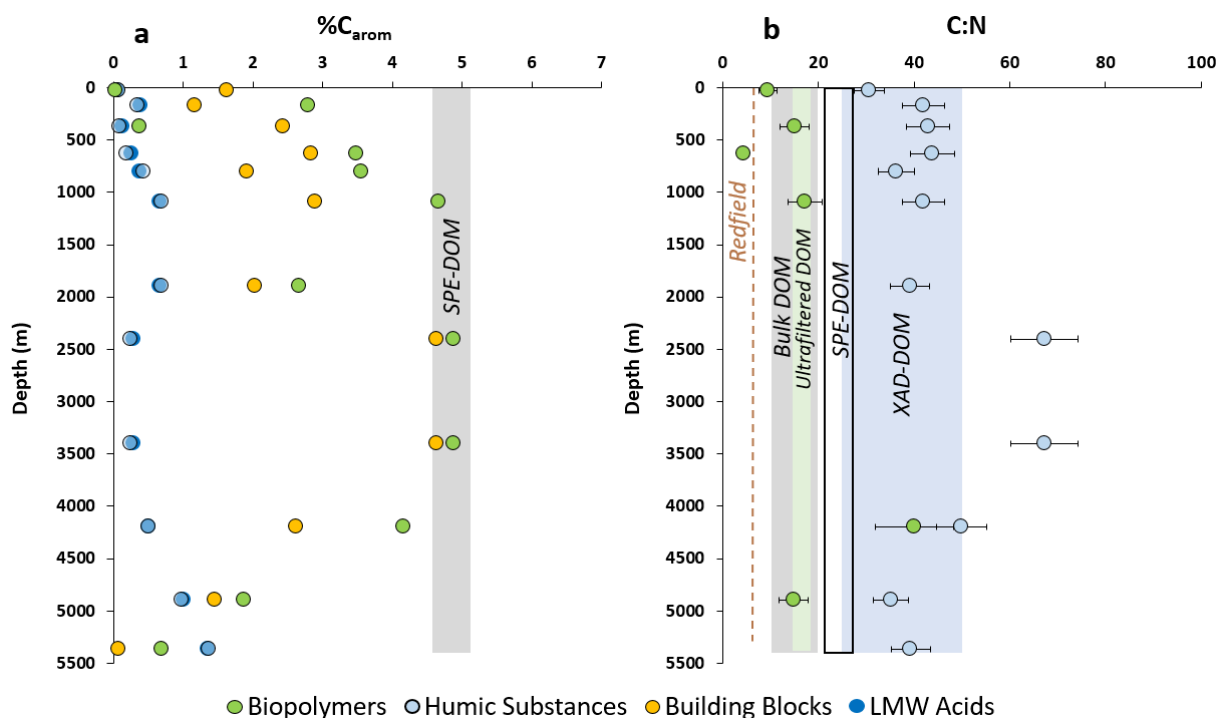


**Figure 4.** (a) Percentage of aromatic carbon against depth (m) measured in four of the five fractions defined by SEC. Aromatic signal was undetectable in the low molecular weight (LMW) neutral fraction. Range of percentage of aromatic carbon in marine SPE-DOM from the Atlantic Ocean (Hertkorn et al., 2013) is also provided for comparison. (b) Elemental C:N ratios measured in the biopolymers (BP) and humic substances (HS) fractions along the water column at 20° 24.431'S, 166° 35.675'W during the TONGA expedition (station 8). Redfield ratio as well as the different ranges of marine C:N ratio in bulk, ultrafiltered, XAD-resin isolated DOM (Hessen & Tranvik, 2013) and SPE-DOM of the Central Pacific Ocean (Green et al., 2014) are provided. Non-visible error bars are covered by the symbols.

472 condensed rings, ultra-refractory to biodegradation (Dittmar, 2008; Marques et al., 2017;  
 473 Nakane et al., 2017; Wagner et al., 2018) and can be found under HMW compounds in the  
 474 deep Pacific Ocean (Ziolkowski & Druffel, 2010). The high percentage of aromatic carbon  
 475 measured in the PDW for BP and BB possibly indicates the presence of black carbon of both  
 476 HMW and LMW at these depths, explaining the persistence of these fractions in the PDW.  
 477 Deeper,  $\%C_{\text{arom}}$  decreases in the water masses containing non-RDOC. This feature suggests  
 478 that the  $\%C_{\text{arom}}$  increases with the refractory nature of BP and BB. The aromaticities of HS  
 479 and LMW acids were significantly lower (0.1 to 1.4% of  $C_{\text{arom}}$ ) than those of BP and BB. The  
 480 extremely low aromatic carbon content of HS contrast with those measured in humic  
 481 standards (e.g. SRFA<sub>2S101F</sub> = 22% $C_{\text{arom}}$ , IHSS) and in estuarine humic-like substances (Riso et  
 482 al., 2021) confirming the difference in the chemical composition of terrestrial and marine HS,  
 483 the latter being known to have extremely low aromaticity (Harvey et al., 1983; Hertkorn et al.,  
 484 2006; Malcolm, 1990; Repeta et al., 2002). The near-zero values in aromatic content  
 485 measured at the surface may result from a production of HS mainly aliphatics together with  
 486 the UV-oxidation of their aromaticity (Corin et al., 1996; Miranda et al., 2020; Zhao et al.,

487 2020). Then, the increase of %C<sub>arom</sub> in the mesopelagic layer down to 2000 m can be  
488 interpreted as a condensation of HS during their biodegradation/transformation by bacteria  
489 into semi-refractory DOM. In the PDW, the %C<sub>arom</sub> of refractory HS was extremely low  
490 (0.25%) and contrasted with the BP and BB fractions. This result possibly indicates that long  
491 term biogeochemical processes occurring in the abyssal waters alter the aromaticity of HS  
492 (aromatic rings and conjugated double bounds) formed in the mesopelagic layer. The  
493 percentage of C<sub>arom</sub> increased again in the younger water masses (LCDW, AABW) found  
494 deeper and close to sediments in line with the occurrence of HS with an advanced state of  
495 biodegradation that are a mix of semi-refractory and refractory HS (Figure 3b).

496 BB are considered as by-products of HS since ultrasonification experiments were conducted  
497 on this DOC fraction (Huber et al., 2011). However, significant correlations were observed  
498 between the %C<sub>arom</sub> of BP and BB ( $R^2 = 0.5408$ ;  $r_s = 0.85$ ) and between HS and LMW acids  
499 ( $R^2 = 0.9895$ ;  $r_s = 0.92$ ). For the two datasets tested, *Spearman* coefficients  $r_s$  close to 1,  
500 further suggesting links existing between these fractions. According to the size-reactivity  
501 continuum, small compounds are produced from the degradation of larger compounds. Based  
502 on the aromatic signature we measured in the fraction, we propose to reconsider the BB as by-  
503 products of the degradation of BP and LMW acids to be generated during the degradation of  
504 HS. This simple definition could then be used to monitor the state of DOM degradation by  
505 following a simple ratio (BP/BB or HS/LMW acids) at large scales. Distribution of the  
506 BP/BB ratio (data not shown) evidenced a global decrease from surface to deep in agreement  
507 with a gradual increase in the state of degradation of DOM with ageing of watermasses.  
508 Based on our measurements, we suggest to no longer consider BB as byproducts of HS, as  
509 initially postulated in Gaid (2011), in open ocean studies. Overall the results of this study lead  
510 to similar conclusions to those obtained from the molecular approach of Osterholz et al.  
511 (2021) that shows a significant increase of the DOM degradation index from surface waters to  
512 the deep layers of the south east oligotrophic Pacific Ocean.

### 513 *C:N elemental ratios in BP and HS*

514 N-content of DOM is of interest to investigate the lability of DOM (Vallino et al., 1996). Due  
515 to the analytical challenge to measure these extremely low organic nitrogen concentrations  
516 studies reporting the C:N ratios of specific DOM compounds in the open ocean are still  
517 scarce. In this work we succeed to measure sub-micromolar organic nitrogen concentrations  
518 in the HS and BP fractions and present the vertical distribution of their respective C:N ratios  
519 (Figure 4b).

520 During the TONGA expedition, the mean C:N ratio in the HS fraction was relatively  
521 homogenous ( $44.7 \pm 4.7$ ;  $n = 12$ ) with the exception of PDW samples wherein the C:N ratio  
522 was significantly higher ( $67.4 \pm 7.1$ ) and can be defined as the C:N ratio of refractory HS. In  
523 the shallowest sample (25 m depth) the C:N ratio of HS was  $30.7 \pm 3.2$ . These values are  
524 higher than those measured in SPE DOM of the Pacific Ocean (21.3 – 27.6; Green et al.,  
525 2014) and lower than those of the *Suwannee River* IHSS standards (e.g. C:N SRFA<sub>2S101F</sub> =  
526 91.1; C:N SRHA<sub>1S101H</sub> = 51.5; IHSS) except for the PDW samples. These values are however  
527 in agreement to the C:N ratios determined in marine HS isolated using XAD resins (Druffel et  
528 al., 1992; Hedges et al., 1992; Lara et al., 1993) including those measured in the open Pacific  
529 Ocean (e.g. 32 – 43, Meyers-Schulte & Hedges, 1986; Hedges et al., 1992). Vertical  
530 variations of the C:N values we measured indicate differences in the bioavailability of  
531 nitrogen and carbon in humic matter. Occurrence of a low C:N ratio ( $30.7 \pm 3.2$ ) at 25 m  
532 depth suggests two pools of humic-like substances, the refractory HS (high C:N) depleted in  
533 nitrogen and the non-refractory HS (low C:N), a N-rich organic matter. Non-refractory HS are  
534 possibly generated during the surface degradation of marine phytoplankton (N-rich) and its  
535 processing by marine bacteria (cellular lysis, microbial transformation). Culture experiments  
536 showing the formation of humic-like compounds (identified by absorbance and fluorescence)  
537 during phytoplankton degradation by bacteria (Osburn et al., 2019) support this pathway of  
538 production. The increase of the C:N elemental ratio with depth indicate a non-redfieldian  
539 mineralization of HS and suggests a preferential remineralization of organic nitrogen  
540 compared to organic carbon.

541 In the BP fraction, C:N ratios (Figure 4b) varied between 4.5 (at 635 m) to 40.1 (at 4198 m).  
542 In the upper 1000 meters depth, the C:N ratios of this fraction fall into the range reported for  
543 ultrafiltered DOM (HMW DOM; 15-18; Hessen & Tranvik, 2013) which is the definition of  
544 BP. In this fraction no organic nitrogen signal can be detected between 1899 m and 3400 m,  
545 indicating that refractory HMW compounds are totally nitrogen depleted in the deep Pacific  
546 Ocean. BP are mainly composed of proteinaceous material in surface water and with only  
547 30% of refractory matter. They can be considered freshly produced and very labile. Absence  
548 of a nitrogen signal in the deep ocean evidences a total utilization of the nitrogen content in  
549 the BP fraction during remineralization. Here again a preferential mineralization of nitrogen  
550 compared to carbon is observed, suggesting that BP is an important nitrogen reservoir for  
551 heterotrophic bacteria. Similar non-redfieldian stoichiometry during DOM mineralization has  
552 already been proposed and modeled (Aminot & K  rouel, 2004; Letscher & Moore, 2015;  
553 Osterholz et al., 2021). Our results confirm the preferential mineralization of nitrogen

554 compared to carbon and suggest that the lability of organic compounds may be tightly linked  
555 to their nitrogen content.

### 556 **3.3 Fluorescent properties of DOM**

557 Fluorescence intensities of three different fluorophores (peaks T, B and M) were measured  
558 along the water column. Measured values largely exceed LOD (see Figure S5), the intensities  
559 and the vertical distributions we report are in agreement with existing data for marine waters  
560 (Tedetti et al., 2011; Yamashita & Tanoue, 2004). Despite the flaws of fluorescence methods,  
561 such as the quenching effect (Chen et al., 2013; Poulin et al., 2014; Yamashita & Jaffé, 2008)  
562 and the ubiquity of some fluorophores (Wünsch et al., 2019), it can provide useful  
563 information on the transformation of DOM in the environment. In this section, we focus on  
564 the vertical distributions of fluorescent indices during the TONGA expedition. Three  
565 fluorescent indices (FI, BIX and HIX) were measured along the water column to further  
566 characterize DOM (Figure 5). These indices were determined based on the works of  
567 McKnight et al. (2001), Huguet et al. (2009) and Zsolnay et al. (1999) respectively. FI is  
568 commonly used to track the DOM sources, in particular to distinguish microbially-derived (FI  
569  $> 1.9$ ) and terrestrially-derived DOM (FI  $< 1.4$ ) in marine waters. Along the water column FI  
570 ranged between 0.2 (5461 m) and 7.0 (370 m). At 25 m and close to the bottom, values were  
571 below 1.4, indicating the existence of a DOM with a FI comparable to terrestrial material. A  
572 low FI close to the sediments may be conceivable however it is unusual in surface waters far  
573 away from terrestrial influence and without terrestrial eolian inputs (monitored using air mass  
574 backward trajectories from the ensemble Hysplit model, [ready.noaa.gov/HYSPLIT.php](http://ready.noaa.gov/HYSPLIT.php)). In  
575 absence of a clear terrestrial influence we relate the low surface FI value to photobleaching.  
576 Photobleaching of FI is not systematic for freshwater DOM (Helms et al., 2014) and, to our  
577 knowledge, has not been reported in marine environment. If proven to be true, the  
578 photobleaching of FI in marine waters have implications for the use of the low FI as a proxy  
579 of terrestrial DOM. A low FI in marine environment should not be systematically assimilated  
580 to a terrestrial influence, especially in environment receiving high solar irradiation (e.g.  
581 subtropical domains). Below the euphotic layer, the FI sharply increased in the mesopelagic  
582 waters to reach  $7.0 \pm 0.4$  and remained high down to 1000 meters depth. These high FI values  
583 suggest the production of microbially-derived DOM (Burdige et al., 2004; Coble 1996) in this  
584 layer (100-1000 m). This increase of FI could be related to the mineralization of a sinking  
585 biomass, produced in the surface, as well as to a microbial transformation of the labile DOM  
586 derived from biomass degradation. The lower values of the FI in the deep sea (Figure 5a)

587 suggest little to no production of microbial DOM below 1089 m (with the exception of FI =  
 588  $2.9 \pm 0.1$  at 3400 m).

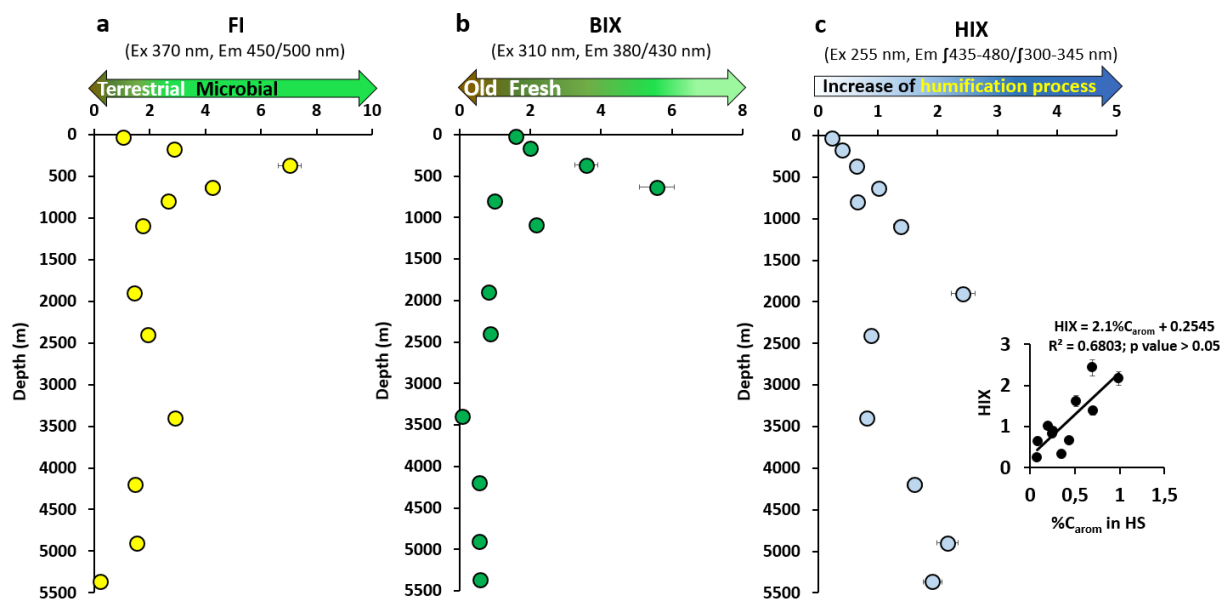


**Figure 5.** Vertical profiles of (a) fluorescence index (FI); (b) biological index (BIX); (c) humification index (HIX) at 20° 24.431'S, 166° 35.675'W during the TONGA expedition (station 8). Nomenclature of index follows those defined by McKnight et al., (2001), Huguet et al., (2009) and Zsolnay et al., (1999) respectively. Insert in (c) shows the significant correlation ( $p$  value = 0.002) recorded between the HIX and the percentage of aromatic carbon in the SEC HS fraction (Figure 4a).

589 The distribution of BIX (Figure 5b) corroborates FI results and provides an estimate of the  
 590 freshness of DOM compounds. A BIX higher than 1 is representative of relatively young  
 591 DOM, produced *in situ*, while a BIX below 0.6 indicates the occurrence of older DOM that  
 592 may suffer from long term processing (e.g. biodegradation, photodegradation, Huguet et al.,  
 593 2009). The BIX values measured ( $0.02 \leq \text{BIX} \leq 5.57$ ) show that DOM can be considered  
 594 relatively young from the surface down to 1089 m, confirming the production of DOM in this  
 595 zone. Abyssal waters had  $\text{BIX} < 1$  implying the presence of old DOM in the deep sea, in  
 596 agreement with the high proportion of RDOM (Figure 3b). Combining FI and BIX results as  
 597 well as the distribution of non-RDOM allowed us to better characterize the dynamics of DOM  
 598 processing in the mesopelagic waters. In the upper 600 meters, the degradation of sinking  
 599 biomass by heterotrophic bacteria produced young HS and BP that were non-refractory and  
 600 N-rich (Figure 3b). These new compounds represented a substantial percentage of DOM.  
 601 Deeper, BB and LMW acids were newly produced (increase of non-refractory percentage) as  
 602 a result of the degradation of the non-refractory BP and HS (Figure 3b). This production of  
 603 BB and LMW acids was observed in the zone (~ 300-700 m) where FI and BIX were  
 604 maximum. These observations suggest that BB and LMW acids could be proxies of microbial  
 605 mineralization products.



606

607 HIX is another indirect proxy of the chemical properties of DOM, highlighting the degree of  
608 humification of organic matter in aquatic environments (Miranda et al., 2018; Zsolnay, 2003).  
609 HIX ranged from 0.24 at 25 m to 2.4 at 1899 m depth (Figure 3c). HIX increased from the  
610 shallow waters ( $0.24 \pm 0.02$ ) to the deep sea ( $\text{HIX} > 1$ ) with the exception of the PDW  
611 wherein relatively low HIX were measured ( $\text{HIX} = 0.88 \pm 0.02$ ). Throughout the water  
612 column, HIX were on average much lower than values measured for vascular plants (1.15 –  
613 4.33; Ohno et al., 2007), soils ( $> 8$ ; Kalbitz et al., 2003), terrestrial aquatic humics from the  
614 IHSS (20 – 50; Birdwell & Engel, 2010) and estuarine and coastal DOM samples ( $\sim 4 - 16$ ;  
615 Huguet et al., 2009). HIX measured in this work were in agreement with those of Chen et al.  
616 (2017) in the Arctic sector of the Pacific Ocean and we propose to define that a HIX below  $\sim$   
617 2.5 indicates a DOM of primarily marine origin. The very low HIX at 25 m depth (Figure 5c)  
618 is in agreement with previous observations in the oligotrophic waters of the Indian Ocean ( $0.9$   
619  $\pm 0.4$ ; Tedetti et al., 2011) and in the Mediterranean Sea ( $0.90 \pm 0.35$  at 5 m depth; Para et al.,  
620 2010). Low HIX in the surface can be related to the phenomenon of photobleaching. Solar  
621 irradiance is known to strongly decrease HIX of DOM in freshwater samples (Helms et al.,  
622 2014; Para et al., 2010) and a similar process was suggested for Mediterranean sea surface  
623 samples (Para et al., 2010). The longterm exposition of marine DOM to solar irradiance and  
624 subsequent fluorescence extinction is the most likely process explaining the low HIX we  
625 measured in the oligotrophic Pacific surface ocean. The increasing values of HIX with depth  
626 across the mesopelagic layer (Figure 5c) suggest a humification of DOM. We relate it to the  
627 transformation of fresh organic matter into an oxidized fluorescent DOM by the microbial  
628 loop. A similar process was previously invoked to explain the increase of the humic-like  
629 fluorescence of DOM in this oceanic basin (Yamashita & Tanoue, 2008; 2009; Yamashita et  
630 al., 2010). According to Paerl et al. (2020), the production of humic-like fluorescent  
631 compounds can also be related to a dimerization of tyrosine catalyzed by peroxidase enzymes  
632 on a short timescale ( $\sim$ hours). During microbial degradation of sinking biomass, this amino-  
633 acid may be released and dimerized by ambient microbial peroxidase therefore increasing  
634 humic-like fluorescence in the mesopelagic waters. HIX often correlates with the aromaticity  
635 of organic matter, as observed in estuarine (Huguet et al., 2009) and soil (Segnini et al., 2010)  
636 samples as well as for humic reference materials (Ateia et al., 2017). The low HIX values we  
637 determined indicate that DOM was poorly aromatic (Birdwell & Engel, 2010) in agreement  
638 with the low aromatic carbon content we measured in the different fractions (Figure 4a).  
639 Similar to previous works, we observed a significant correlation ( $R^2 = 0.6803$ ;  $p$  value  $< 0.05$ )

640 between HIX and %C<sub>arom</sub> in the HS fraction (insert in Figure 5c). This result demonstrates  
641 that the HS fraction operationally defined by SEC is well representative of the humic material.  
642 Such simultaneous increase of HIX and aromaticity has been observed during microbial  
643 degradation experiments of soil organic matter (Kalbitz et al., 2003). Moreover, there is recent  
644 evidence that HIX increases during the microbial degradation of phytoplankton biomass  
645 (Kinsey et al., 2018), indicating that microbial processing also controls the humification of  
646 DOM in marine systems. Low HIX in the older PDW are consistent with the low aromatic  
647 carbon content of HS (Figure 5a) further suggesting an alteration of aromaticity with ageing  
648 of refractory humic matter. The increase of HIX in the deepest samples (Figure 5c) is likely  
649 representative of the mixing between watermasses formed in different areas with DOM  
650 content of different ages and thus of different degrees of decomposition. Finally, the  
651 concomitant increase of humic-like fluorescence (e.g. peak M, Figure S5 and HIX Figure 5c)  
652 and decrease of humic-like carbon evidence a gain of fluorescence quantum yield by the  
653 humic material during its microbial processing in the mesopelagic waters. Fluorescence  
654 spectroscopy is thereby useful to identify the humification process but not to quantify the  
655 fraction of DOC related to humic matter in marine environments.

656  
657 Our results show that fluorescence data are usable proxies for the study of DOM  
658 bioavailability when associated to quantitative DOM data ([DOC] and %C<sub>arom</sub> in the isolated  
659 fractions). In this work, the use of this combination on field samples confirms experimental  
660 observations during heterotrophic bacteria incubations (Zheng et al., 2019). Microbial ageing  
661 of a relatively labile DOM, originating from oligotrophic phytoplankton, induces the  
662 consumption of a low aromatic DOM with a low humic-like fluorescent signature and its  
663 transformation to RDOM displaying a high humic-like fluorescence signature and enriched in  
664 aromatic carbon.

### 665 **3.4 Iron binding properties of oceanic humic substances**

666 We further characterized the chemical properties of HS in the WTSP by determining their  
667 electroactivity and thereby their complexing capacity for dFe. The concentrations of eHS  
668 ranged from 23.2 to 160.2  $\mu\text{g-eqSRFA L}^{-1}$  (Figure 6a).

669 These concentrations are in agreement with those reported in other marine environments  
670 including the Pacific Ocean (Cabanes et al., 2020; Dulaquais et al., 2018a; Laglera et al.,  
671 2019; Whitby et al., 2020a). The vertical distribution of eHS displays the typical profile  
672 reported in these previous studies, with a surface enrichment and low concentrations in the  
673 deep sea. The surface enrichment can be related to a production of eHS during bacterial

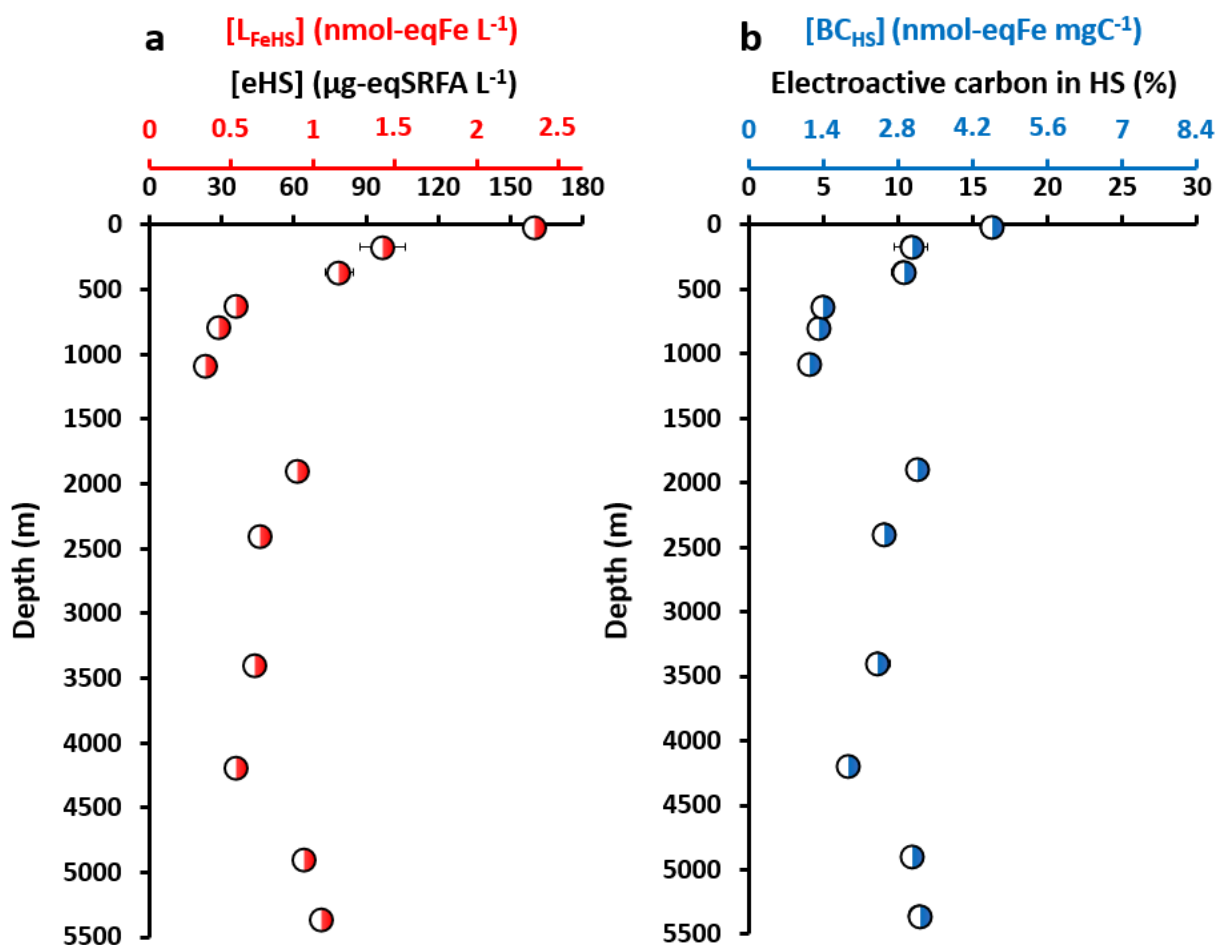


**Figure 6.** Vertical distributions of the concentrations of (a) electroactive humic substances (eHS, expressed in  $\mu\text{g-eqSRFA L}^{-1}$ ) and humic-type ligands ( $L_{\text{FeHS}}$ ) expressed in  $\text{nmol-eqFe L}^{-1}$  (calculated following Dulaquais et al., 2018b and Sukekava et al., 2018); (b) the percentage of electroactive carbon in the HS fraction along with the binding capacity of humic carbon for iron ( $BC_{\text{HS}}$  expressed in  $\text{nmol-eqFe mgC}^{-1}$ ) at  $20^{\circ} 24.431'S$ ,  $166^{\circ} 35.675'W$  at the TONGA station.

674 degradation of the biomass as previously demonstrated by Whitby et al. (2020a). High surface  
675 eHS concentrations and their decrease with depth in the mesopelagic layer suggest that the  
676 electroactivity of humic matter is a property affected by all the biogeochemical processes  
677 governing the distribution of HS (e.g. surface production, bacterial degradation). The deep sea  
678 concentrations of eHS were quite homogeneous ( $50 \pm 12 \mu\text{g-eqSRFA L}^{-1}$ ) indicating a partial  
679 recalcitrance of the electroactivity to long term degradation. Conversion of eHS (in  $\mu\text{g-}$   
680  $\text{eqSRFA L}^{-1}$ ) into Fe-binding ligands of humic type ( $L_{\text{FeHS}}$ ) can be estimated using the binding  
681 capacity of the model humic-type ligand SRFA (1S101F) for dFe in seawater ( $14.6 \pm 0.7$   
682  $\text{nmolFe mgSRFA}^{-1}$ ; Sukekava et al., 2018). A similar conversion is commonly used in the  
683 recent literature (Dulaquais et al., 2018a, 2020; Laglera et al., 2019; Whitby et al., 2020a). At  
684 this station we estimated  $L_{\text{FeHS}}$  values of between 0.3 and  $2.4 \text{ nmol-eqFe L}^{-1}$ . This interval fell  
685 into the range of Fe-binding ligand ( $L_{\text{Fe}}$ ) concentrations previously measured in the south

686 oligotrophic Pacific Ocean ( $0 - 4 \text{ nmol-eqFe L}^{-1}$ ; Buck et al., 2018; Cabanes et al., 2020).  
687 This result demonstrates that part of  $L_{\text{Fe}}$  were of humic nature.  
688 In the oligotrophic Pacific Ocean, dFe is extremely depleted in surface waters ( $\leq 0.1 \text{ nM}$ ,  
689 Buck et al., 2018; Cabanes et al., 2020; Guieu et al., 2018). The implication of  $L_{\text{FeHS}}$  in the  
690 stabilization of surface dFe can be considered limited due to the possible occurrence of very  
691 strong iron binding ligands in this layer (e.g. siderophores, Boiteau et al., 2016). In contrast,  
692 in the deep ocean ( $> 1000 \text{ m}$ ) dFe exists at higher concentrations ( $> 0.4 \text{ nM}$ ). At these depths,  
693 intermediate iron chelators dominate (called  $L_2$  in Buck et al., 2018) and humic-type ligands  
694 are thought to be a major component of this class of ligand (Bundy et al., 2015), therefore the  
695 role of humics in the stabilization of dFe is probably enhanced in the deep Pacific Ocean. To  
696 monitor the modifications of the binding properties of HS along with biogeochemical  
697 processes we determined the contribution of eHS to the HS fraction defined by SEC and  
698 estimated the binding capacity for Fe of humic DOC ( $\text{BC}_{\text{HS}}$ , Figure 6b). This calculation  
699 considers the carbon content of the SRFA standard used (52.44%) to normalize the  
700 concentrations expressed in  $\mu\text{g eq-SRFA L}^{-1}$  into  $\mu\text{gC L}^{-1}$  and assumes that all eHS elute in  
701 the HS fraction operationally defined by SEC (Riso et al., 2021). At this station the average  
702 contribution of eHS to the total HS carbon was  $\sim 9.1 \pm 0.6 \%$  (Figure 6b). This contribution  
703 varied along the water column with a maximum at 25 m (16.2%) and a minimum at 1089 m  
704 (4.1%). The non-constant contribution of eHS to HS DOC implies a non-conservativity of the  
705 binding properties of HS during their biogeochemical processing.  
706 The  $\text{BC}_{\text{HS}}$  were systematically below those of the SRFA standard ( $\text{BC}_{\text{SRFA}} = 27.8 \pm 1.3 \text{ nmol-}$   
707  $\text{eqFe mgC}^{-1}$ ) indicating a lower BC of marine humic carbon compared to the terrigenous  
708 humic matter.  $\text{BC}_{\text{HS}}$  in the shallowest sample ( $4.5 \pm 0.1 \text{ nmol-eqFe mgC}^{-1}$ ) was significantly  
709 higher than in the deep sea ( $2.7 \pm 0.5 \text{ nmol-eqFe mgC}^{-1}$ ;  $n = 6$ ). A large part of HS in the  
710 upper 100 m depths was non-refractory (50%; Figure 3b), thereby we deduce that the binding  
711 capacity for dFe of non-refractory HS is higher than that of refractory HS. The decrease of the  
712  $\text{BC}_{\text{HS}}$  from surface to 1089 m and the strong decrease of the contribution of eHS to humic  
713 DOC in the mesopelagic waters (Figure 6b) indicate an alteration of the Fe-binding properties  
714 during the microbial mineralization of HS DOC. Statistical analysis of the data did not reveal  
715 significant correlations between  $\text{BC}_{\text{HS}}$ ,  $\%C_{\text{arom}}$  nor the C:N elemental ratio of HS. This result  
716 suggests that Fe-binding moieties of marine HS are aliphatic and that the N-containing  
717 functional groups may not be involved in the formation of the Fe-humic complex in the  
718 marine environment. Based on these results, we suspect carboxylates to be the main chemical  
719 functional group involved in the Fe-binding properties of oceanic HS. Carboxylates are of

720 intermediate strength (Bundy et al., 2015) compared to N-containing (strong, Gledhill &  
721 Buck, 2012; Rue & Bruland, 1995) and aromatic/phenolic (weak, González et al., 2019)  
722 moieties for Fe complexation. The correlation between Fe-binding HS and CRAM in  
723 estuarine samples (Bundy et al., 2015) and the observations of humic type ligands falling into  
724 the intermediate class of Fe chelators (Buck et al., 2018; Bundy et al., 2015) both support this  
725 hypothesis. The decrease of  $BC_{HS}$  in the mesopelagic waters can be interpreted as a decrease  
726 of the abundance of carboxylates with HS during microbial transformation. This latter  
727 hypothesis is supported by the long-term experimental study (1 year) on the degradation of a  
728 large size spectra of DOM (108-7410 Da) by marine bacteria from Daoud & Trembley  
729 (2019). Their study showed a substantial decrease of carboxylate abundance in seawater  
730 DOM that suffered from microbial degradation compared to the control sample. There is  
731 currently no NMR data on oceanic HS samples to confirm this and the acquisition of such  
732 data along a full water column in the future would allow for the testing of this hypothesis.  
733 Our results and interpretations of the complexation of dFe by humic matter contrast with  
734 terrestrial HS. For terrestrial HS, the binding capacity for dFe is thought to be linked to their  
735 aromaticity (Kikuchi et al., 2017) as it is observed in the two most used humic type standards  
736 SRFA ( $\%C_{arom} = 24\%$ ;  $BC_{SRFA\ 1S101F} = 14.6\ \text{nmolFe mgSRFA}^{-1}$ ; Sukekava et al., 2018) and  
737 SRHA ( $\%C_{arom} = 37\%$ ;  $BC_{SRHA\ 1S101H} = 31\text{-}32\ \text{nmolFe mgSRHA}^{-1}$ ; Abualhaija & van den  
738 Berg, 2014; Laglera & van den Berg, 2009). This difference further denotes the uniqueness of  
739 marine HS compared to terrestrial humic matter, as previously discussed by Malcolm (1990)  
740 in terms of chemical properties. We note that our results also contrast with Whitby et al.  
741 (2020b) where it was hypothesised that the Fe-binding capacities increased with depth due to  
742 higher HS aromaticity. In their study the higher Fe-binding capacities of HS in deep waters of  
743 the North Atlantic could be a result of a high fraction of terrestrial HS, in part derived from  
744 the subduction of humic-rich Arctic waters, which have been shown to have particularly high  
745 Fe-HS stability constants (Laglera et al., 2019). Lignin, an unambiguous molecular tracer for  
746 terrestrial DOC, is also higher in the Atlantic Ocean than in the Pacific Ocean (Hernes &  
747 Benner, 2002, 2006; Opsahl & Benner 1997). This suggests that the contribution of HS from  
748 terrestrial vs. marine sources could result in differences in Fe-complexing behaviour between  
749 oceanic regions.

#### 750 **4. Conclusions**

751 This work presents the opportunity provided by multi-detection SEC to study the size-  
752 reactivity continuum and the chemical properties of oceanic DOC without any prior

753 extraction. This method has an excellent recovery of DOC and requires only a small sample  
754 volume (2.5 mL).

755 We used a combination of three semi-specific methods (SEC, fluorescence, CSV) to study  
756 DOM chemical modifications induced by biogeochemical processes along the water column  
757 of the oligotrophic Pacific Ocean. We identified N-contents of the BP and HS fractions as  
758 pools of bioavailable nitrogen. Our results also suggest the condensation, the decrease in N-  
759 content, the increase of quantum yield of fluorescence and a loss of complexing capacity for  
760 dFe of HS during microbial degradation of DOM. Marine HS seem to be produced in surface  
761 waters during biomass degradation. HS are initially non-refractory, nevertheless their ageing  
762 induces their transformation into refractory DOM. This process was identified to occur in two  
763 steps. First the microbial transformation in the mesopelagic waters increases their aromaticity  
764 and their fluorescence, secondly, long term (> centuries) processing alters their aromatic  
765 content making marine HS more aliphatic. All these changes in the chemical properties could  
766 alter and gradually degrade the newly produced labile DOM into RDOM trapped in the deep  
767 ocean. This work provides insights to reconcile the quantitative (loss of matter) and  
768 qualitative (increase of fluorescence) views in humic oceanic biogeochemistry.

769 Results of this work and the conclusions drawn are consistent with studies that used molecular  
770 approaches to characterize fate of DOM in field samples (Osterholz et al., 2021) and in  
771 bacterial incubation experiments (Lian et al., 2021; Zheng et al., 2019). A larger scale study  
772 and the use of a molecular approach to each DOM fraction isolated in this work would  
773 confirm the main hypotheses.

#### 774 **Acknowledgments**

775 We would like to thank Vincent Taillandier for providing CTD data for the TONGA GPpr14  
776 cruise. CTD data from the TONGA expedition are available at [http://www.obs-  
778 vlfr.fr/proof/php/TONGA/tonga.php](http://www.obs-<br/>777 vlfr.fr/proof/php/TONGA/tonga.php). We acknowledge the dedicated sea-going staff of the  
779 Ocean Data Facility of S.I.O for generating high quality and calibrated CTD data during the  
780 US-GP15 expedition. CTD data from the US-GP15 cruise are available at  
781 <https://cchdo.ucsd.edu/cruise/33RR20180918>. CTD data from the CLIVAR-P16 expedition  
782 are available at <https://www.bco-dmo.org/dataset/778403>. We warmly thank captains and  
783 crew of R/V *L'Atalante* and *Roger Revelle*, as well as chief scientists Karen Casciotti, Greg  
784 Cutter & Phoebe Lam of the US-GP15 expedition, Cécile Guieu & Sophie Bonnet of the  
785 TONGA expedition, and the scientific crews of both expeditions for their work at sea and  
786 sample collection. We especially thank Matthieu Bressac, Veronica Arnone and David  
786 González-Santana for sampling during the TONGA cruise. We are grateful to Karen Casciotti

787 for her valuable assistance to get GEOTRACES samples. We warmly thank Pascal Annabelle  
788 Baya for subsampling of GEOTRACES samples. We also thank the PACEM platform for the  
789 Mediterranean Institute of Oceanography. We thank Millie Goddard-Dwyer for assistance in  
790 editing and reviewing. This work is part of the BioDOMPO project (PI. Gabriel Dulaquais),  
791 funded by the French National program LEFE (*Les enveloppes Fluides et l'Environnement*)  
792 Cyber of the CNRS and ISblue ([www.isblue.fr](http://www.isblue.fr)). This work is part of the TONGA project  
793 (ANR-18-CE1-0016, CNRS, IRD, Ifremer). The PhD grant of Pierre Fourier was funded by  
794 ISblue and région Bretagne. This work was conducted in the framework of the GEOTRACES  
795 program.

796

## 797 **References**

- 798 Abualhaija, M. M., & van den Berg, C. M. (2014). Chemical speciation of iron in seawater using catalytic  
799 cathodic stripping voltammetry with ligand competition against salicylaldoxime. *Marine Chemistry*, 164, 60-74.  
800 <https://doi.org/10.1016/j.marchem.2014.06.005>.
- 801 Aiken, G. R., Brown, P. A., Noyes, T. I., & Pinckney, D. J. (1989). Molecular size and weight of fulvic and  
802 humic acids from the Suwannee River. *Humic substances in the Suwannee River, Georgia: Interactions,*  
803 *properties, and proposed structures*, 87-557.
- 804 Aminot, A., & K erouel, R. (2004). Dissolved organic carbon, nitrogen and phosphorus in the NE Atlantic and  
805 the NW Mediterranean with particular reference to non-refractory fractions and degradation. *Deep Sea Research*  
806 *Part I: Oceanographic Research Papers*, 51(12), 1975-1999. <https://doi.org/10.1016/j.dsr.2004.07.016>
- 807 Amon, R. M., & Benner, R. (1994). Rapid cycling of high-molecular-weight dissolved organic matter in the  
808 ocean. *Nature*, 369(6481), 549-552. <https://doi.org/10.1038/369549a0>
- 809 Amon, R. M., & Benner, R. (1996). Bacterial utilization of different size classes of dissolved organic matter.  
810 *Limnology and Oceanography*, 41(1), 41-51. <https://doi.org/10.4319/lo.1996.41.1.0041>
- 811 Amy, G., & Her, N. (2004). Size exclusion chromatography (SEC) with multiple detectors: a powerful tool in  
812 treatment process selection and performance monitoring. *Water science and technology: Water supply*, 4(4), 19-  
813 24. <https://doi.org/10.2166/ws.2004.0056>
- 814 Arrieta, J. M., Mayol, E., Hansman, R. L., Herndl, G. J., Dittmar, T., & Duarte, C. M. (2015). Dilution limits  
815 dissolved organic carbon utilization in the deep ocean. *Science*, 348(6232), 331-333.  
816 <https://doi.org/10.1126/science.1258955>
- 817 Ateia, M., Ran, J., Fujii, M., & Yoshimura, C. (2017). The relationship between molecular composition and  
818 fluorescence properties of humic substances. *International Journal of Environmental Science and Technology*,  
819 14(4), 867-880. <https://doi.org/10.1007/s13762-016-1214-x>
- 820 Baghoth, S. A., Maeng, S. K., Rodriguez, S. S., Ronteltap, M., Sharma, S., Kennedy, M., & Amy, G. L. (2008).  
821 An urban water cycle perspective of natural organic matter (NOM): NOM in drinking water, wastewater  
822 effluent, storm water, and seawater. *Water Science and Technology: Water Supply*, 8(6), 701-707.  
823 <https://doi.org/10.2166/ws.2008.146>
- 824 Becker, S. & Swift, J. 2020. CTD data from Cruise 33RR20180918, exchange version. Accessed from CCHDO  
825 <https://cchdo.ucsd.edu/cruise/33RR20180918>. Access date 2021-01-05.
- 826 Benner, R. (2003). Molecular indicators of the bioavailability of dissolved organic matter. In *Aquatic ecosystems*  
827 (pp. 121-137). Academic Press. <https://doi.org/10.1016/B978-012256371-3/50006-8>

- 828 Benner, R., & Amon, R. M. (2015). The size-reactivity continuum of major bioelements in the ocean. Annual  
829 review of marine science, 7, 185-205. <https://doi.org/10.1146/annurev-marine-010213-135126>
- 830 Bercovici, S. K., & Hansell, D. A. (2016). Dissolved organic carbon in the deep Southern Ocean: Local versus  
831 distant controls. *Global Biogeochemical Cycles*, 30(2), 350-360. <https://doi.org/10.1002/2015GB005252>
- 832 Birdwell, J. E., & Engel, A. S. (2010). Characterization of dissolved organic matter in cave and spring waters  
833 using UV-Vis absorbance and fluorescence spectroscopy. *Organic Geochemistry*, 41(3), 270-280.  
834 <https://doi.org/10.1016/j.orggeochem.2009.11.002>
- 835 Boiteau, R. M., Mende, D. R., Hawco, N. J., McIlvin, M. R., Fitzsimmons, J. N., Saito, M. A., ... & Repeta, D. J.  
836 (2016). Siderophore-based microbial adaptations to iron scarcity across the eastern Pacific Ocean. *Proceedings*  
837 *of the National Academy of Sciences*, 113(50), 14237-14242. <https://doi.org/10.1073/pnas.1608594113>
- 838 Buck, K. N., Sedwick, P. N., Sohst, B., & Carlson, C. A. (2018). Organic complexation of iron in the eastern  
839 tropical South Pacific: results from US GEOTRACES Eastern Pacific Zonal Transect (GEOTRACES cruise  
840 GP16). *Marine Chemistry*, 201, 229-241. <https://doi.org/10.1016/j.marchem.2017.11.007>
- 841 Bundy, R. M., Abdulla, H. A., Hatcher, P. G., Biller, D. V., Buck, K. N., & Barbeau, K. A. (2015). Iron-binding  
842 ligands and humic substances in the San Francisco Bay estuary and estuarine-influenced shelf regions of coastal  
843 California. *Marine Chemistry*, 173, 183-194. <https://doi.org/10.1016/j.marchem.2014.11.005>
- 844 Burdige, D. J., Kline, S. W., & Chen, W. (2004). Fluorescent dissolved organic matter in marine sediment pore  
845 waters. *Marine Chemistry*, 89(1-4), 289-311. <https://doi.org/10.1016/j.marchem.2004.02.015>
- 846 Cabanes, D. J., Norman, L., Bowie, A. R., Strmečki, S., & Hassler, C. S. (2020). Electrochemical evaluation of  
847 iron-binding ligands along the Australian GEOTRACES southwestern Pacific section (GP13). *Marine*  
848 *Chemistry*, 219, 103736. <https://doi.org/10.1016/j.marchem.2019.103736>
- 849
- 850 Chen, M., & Hur, J. (2015). Pre-treatments, characteristics, and biogeochemical dynamics of dissolved organic  
851 matter in sediments: A review. *water research*, 79, 10-25. <https://doi.org/10.1016/j.watres.2015.04.018>
- 852 Chen, W. B., Smith, D. S., & Guéguen, C. (2013). Influence of water chemistry and dissolved organic matter  
853 (DOM) molecular size on copper and mercury binding determined by multiresponse fluorescence quenching.  
854 *Chemosphere*, 92(4), 351-359. <https://doi.org/10.1016/j.chemosphere.2012.12.075>
- 855 Chen, M., Nam, S. I., Kim, J. H., Kwon, Y. J., Hong, S., Jung, J., ... & Hur, J. (2017). High abundance of  
856 protein-like fluorescence in the Amerasian Basin of Arctic Ocean: Potential implication of a fall phytoplankton  
857 bloom. *Science of the Total Environment*, 599, 355-363. <https://doi.org/10.1016/j.scitotenv.2017.04.233>
- 858 Coble, P. G. (1996). Characterization of marine and terrestrial DOM in seawater using excitation-emission  
859 matrix spectroscopy. *Marine chemistry*, 51(4), 325-346. [https://doi.org/10.1016/0304-4203\(95\)00062-3](https://doi.org/10.1016/0304-4203(95)00062-3)
- 860 Coble, P. G. (2007). Marine optical biogeochemistry: the chemistry of ocean color. *Chemical reviews*, 107(2),  
861 402-418. <https://doi.org/10.1021/cr050350+>
- 862 Coppola, A. I., & Druffel, E. R. (2016). Cycling of black carbon in the ocean. *Geophysical Research Letters*,  
863 43(9), 4477-4482. <https://doi.org/10.1002/2016GL068574>
- 864 Corin, N., Backlund, P., & Kulovaara, M. (1996). Degradation products formed during UV-irradiation of humic  
865 waters. *Chemosphere*, 33(2), 245-255. [https://doi.org/10.1016/0045-6535\(96\)00167-1](https://doi.org/10.1016/0045-6535(96)00167-1)
- 866 Cornelissen, E. R., Moreau, N., Siegers, W. G., Abrahamse, A. J., Rietveld, L. C., Grefte, A., ... & Wessels, L. P.  
867 (2008). Selection of anionic exchange resins for removal of natural organic matter (NOM) fractions. *Water*  
868 *research*, 42(1-2), 413-423. <https://doi.org/10.1016/j.watres.2007.07.033>
- 869 Cutter, G. A., Scientists, C. C., Casciotti, K. L., & Lam, P. J. (2018). US GEOTRACES Pacific Meridional  
870 Transect-GP15 Cruise Report.



- 871 Daoud, A. B. A., & Tremblay, L. (2019). HPLC-SEC-FTIR characterization of the dissolved organic matter  
872 produced by the microbial carbon pump. *Marine Chemistry*, 215, 103668.  
873 <https://doi.org/10.1016/j.marchem.2019.103668>
- 874 Del Vecchio, R., & Blough, N. V. (2002). Photobleaching of chromophoric dissolved organic matter in natural  
875 waters: kinetics and modeling. *Marine Chemistry*, 78(4), 231-253. [https://doi.org/10.1016/S0304-4203\(02\)00036-1](https://doi.org/10.1016/S0304-4203(02)00036-1)  
876
- 877 Dhakal, N., Salinas-Rodriguez, S. G., Ouda, A., Schippers, J. C., & Kennedy, M. D. (2018). Fouling of  
878 ultrafiltration membranes by organic matter generated by marine algal species. *Journal of Membrane Science*,  
879 555, 418-428. <https://doi.org/10.1016/j.memsci.2018.03.057>
- 880 Dittmar, T. (2008). The molecular level determination of black carbon in marine dissolved organic matter.  
881 *Organic Geochemistry*, 39(4), 396-407. <https://doi.org/10.1016/j.orggeochem.2008.01.015>
- 882 Dittmar, T., & Kattner, G. (2003). The biogeochemistry of the river and shelf ecosystem of the Arctic Ocean: a  
883 review. *Marine chemistry*, 83(3-4), 103-120. [https://doi.org/10.1016/S0304-4203\(03\)00105-1](https://doi.org/10.1016/S0304-4203(03)00105-1)
- 884 Dittmar, T., & Koch, B. P. (2006). Thermogenic organic matter dissolved in the abyssal ocean. *Marine*  
885 *Chemistry*, 102(3-4), 208-217. <https://doi.org/10.1016/j.marchem.2006.04.003>
- 886 Dittmar, T., & Paeng, J. (2009). A heat-induced molecular signature in marine dissolved organic matter. *Nature*  
887 *Geoscience*, 2(3), 175-179. <https://doi.org/10.1038/ngeo440>
- 888 Druffel, E. R., Williams, P. M., Bauer, J. E., & Ertel, J. R. (1992). Cycling of dissolved and particulate organic  
889 matter in the open ocean. *Journal of Geophysical Research: Oceans*, 97(C10), 15639-15659.  
890 <https://doi.org/10.1029/92JC01511>
- 891 Dulaquais, G., Breitenstein, J., Waeles, M., Marsac, R., & Riso, R. (2018b). Measuring dissolved organic matter  
892 in estuarine and marine waters: size-exclusion chromatography with various detection methods. *Environmental*  
893 *Chemistry*, 15(7), 436-449. <https://doi.org/10.1071/EN18108>
- 894 Dulaquais, G., Waeles, M., Breitenstein, J., Knoery, J., & Riso, R. (2020). Links between size fractionation,  
895 chemical speciation of dissolved copper and chemical speciation of dissolved organic matter in the Loire estuary.  
896 *Environmental Chemistry*, 17(5), 385-399. <https://doi.org/10.1071/EN19137>
- 897 Dulaquais, G., Waeles, M., Gerringa, L. J., Middag, R., Rijkenberg, M. J., & Riso, R. (2018a). The  
898 biogeochemistry of electroactive humic substances and its connection to iron chemistry in the North East  
899 Atlantic and the Western Mediterranean Sea. *Journal of Geophysical Research: Oceans*, 123(8), 5481-5499.  
900 <https://doi.org/10.1029/2018JC014211>
- 901 Ertel, J. R., Hedges, J. I., & Perdue, E. M. (1984). Lignin signature of aquatic humic substances. *Science*,  
902 223(4635), 485-487. <https://doi.org/10.1126/science.223.4635.485>
- 903 Esteves, V. I., Otero, M., & Duarte, A. C. (2009). Comparative characterization of humic substances from the  
904 open ocean, estuarine water and fresh water. *Organic Geochemistry*, 40(9), 942-950.  
905 <https://doi.org/10.1016/j.orggeochem.2009.06.006>
- 906 Fellman, J. B., Hood, E., & Spencer, R. G. (2010). Fluorescence spectroscopy opens new windows into  
907 dissolved organic matter dynamics in freshwater ecosystems: A review. *Limnology and oceanography*, 55(6),  
908 2452-2462. <https://doi.org/10.4319/lo.2010.55.6.2452>
- 909 Fichot, C. G., & Benner, R. (2011). A novel method to estimate DOC concentrations from CDOM absorption  
910 coefficients in coastal waters. *Geophysical research letters*, 38(3). <https://doi.org/10.1029/2010GL046152>
- 911 Fumenia, A., Moutin, T., Bonnet, S., Benavides, M., Petrenko, A., Helias Nunige, S., & Maes, C. (2018). Excess  
912 nitrogen as a marker of intense dinitrogen fixation in the Western Tropical South Pacific Ocean: impact on the  
913 thermocline waters of the South Pacific. *Biogeosciences Discussions*, 1-33. <https://doi.org/10.5194/bg-2017-557>

- 914 Gaid, K. (2011). A Large Review of Pretreatment. *Expanding issues in desalination*.  
915 <https://doi.org/10.5772/19680>
- 916 Gao, Z., & Guéguen, C. (2018). Distribution of thiol, humic substances and colored dissolved organic matter  
917 during the 2015 Canadian Arctic GEOTRACES cruises. *Marine Chemistry*, 203, 1-9.  
918 <https://doi.org/10.1016/j.marchem.2018.04.001>
- 919 Gledhill, M., & Buck, K. N. (2012). The organic complexation of iron in the marine environment: a review.  
920 *Frontiers in microbiology*, 3, 69. <https://doi.org/10.3389/fmicb.2012.00069>
- 921 González, A. G., Cadena-Aizaga, M. I., Sarthou, G., González-Dávila, M., & Santana-Casiano, J. M. (2019).  
922 Iron complexation by phenolic ligands in seawater. *Chemical geology*, 511, 380-388.  
923 <https://doi.org/10.1016/j.chemgeo.2018.10.017>
- 924 Green, N. W., Perdue, E. M., Aiken, G. R., Butler, K. D., Chen, H., Dittmar, T., ... & Stubbins, A. (2014). An  
925 intercomparison of three methods for the large-scale isolation of oceanic dissolved organic matter. *Marine*  
926 *Chemistry*, 161, 14-19. <https://doi.org/10.1016/j.marchem.2014.01.012>
- 927 Gu, B., Schmitt, J., Chen, Z., Liang, L., & McCarthy, J. F. (1995). Adsorption and desorption of different  
928 organic matter fractions, on iron oxide. *Geochimica et cosmochimica acta*, 59(2), 219-229.  
929 [https://doi.org/10.1016/0016-7037\(94\)00282-Q](https://doi.org/10.1016/0016-7037(94)00282-Q)
- 930 Guieu, C., Bonnet, S. (2019). TONGA Cruise Report. <https://doi.org/10.17600/18000884>
- 931 Guieu, C., Bonnet, S., Petrenko, A., Menkes, C., Chavagnac, V., Desboeufs, K., ... & Moutin, T. (2018). Iron  
932 from a submarine source impacts the productive layer of the Western Tropical South Pacific (WTSP). *Scientific*  
933 *reports*, 8(1), 1-9. <https://doi.org/10.1073/pnas.1619514114>
- 934 Hach, P. F., Marchant, H. K., Krupke, A., Riedel, T., Meier, D. V., Lavik, G., ... & Kuypers, M. M. (2020).  
935 Rapid microbial diversification of dissolved organic matter in oceanic surface waters leads to carbon  
936 sequestration. *Scientific reports*, 10(1), 1-10. <https://doi.org/10.1038/s41598-020-69930-y>
- 937 Hansell, D. A., Carlson, C. A., Repeta, D. J., & Schlitzer, R. (2009). Dissolved organic matter in the ocean: A  
938 controversy stimulates new insights. *Oceanography*, 22(4), 202-211. <https://doi.org/10.5670/oceanog.2009.109>
- 939 Hartin, C. A., Fine, R. A., Sloyan, B. M., Talley, L. D., Chereskin, T. K., & Happell, J. (2011). Formation rates  
940 of Subantarctic mode water and Antarctic intermediate water within the South Pacific. *Deep Sea Research Part*  
941 *I: Oceanographic Research Papers*, 58(5), 524-534. <https://doi.org/10.1016/j.dsr.2011.02.010>
- 942 Harvey, G. R., Boran, D. A., Chesal, L. A., & Tokar, J. M. (1983). The structure of marine fulvic and humic  
943 acids. *Marine Chemistry*, 12(2-3), 119-132. [https://doi.org/10.1016/0304-4203\(83\)90075-0](https://doi.org/10.1016/0304-4203(83)90075-0)
- 944 Hawco, N. J., Lam, P. J., Lee, J. M., Ohnemus, D. C., Noble, A. E., Wyatt, N. J., ... & Saito, M. A. (2018).  
945 Cobalt scavenging in the mesopelagic ocean and its influence on global mass balance: Synthesizing water  
946 column and sedimentary fluxes. *Marine Chemistry*, 201, 151-166.  
947 <https://doi.org/10.1016/j.marchem.2017.09.001>
- 948 Hedges, J. I., Hatcher, P. G., Ertel, J. R., & Meyers-Schulte, K. J. (1992). A comparison of dissolved humic  
949 substances from seawater with Amazon River counterparts by <sup>13</sup>C-NMR spectrometry. *Geochimica et*  
950 *Cosmochimica Acta*, 56(4), 1753-1757. [https://doi.org/10.1016/0016-7037\(92\)90241-A](https://doi.org/10.1016/0016-7037(92)90241-A)
- 951 Helms, J. R., Mao, J., Stubbins, A., Schmidt-Rohr, K., Spencer, R. G., Hernes, P. J., & Mopper, K. (2014). Loss  
952 of optical and molecular indicators of terrigenous dissolved organic matter during long-term photobleaching.  
953 *Aquatic sciences*, 76(3), 353-373. <https://doi.org/10.1007/s00027-014-0340-0>
- 954 Helms, J. R., Stubbins, A., Perdue, E. M., Green, N. W., Chen, H., & Mopper, K. (2013). Photochemical  
955 bleaching of oceanic dissolved organic matter and its effect on absorption spectral slope and fluorescence.  
956 *Marine Chemistry*, 155, 81-91. <https://doi.org/10.1016/j.marchem.2013.05.015>

- 957 Hernes, P. J., & Benner, R. (2002). Transport and diagenesis of dissolved and particulate terrigenous organic  
 958 matter in the North Pacific Ocean. *Deep Sea Research Part I: Oceanographic Research Papers*, 49(12), 2119-  
 959 2132. [https://doi.org/10.1016/S0967-0637\(02\)00128-0](https://doi.org/10.1016/S0967-0637(02)00128-0)
- 960 Hernes, P. J., & Benner, R. (2006). Terrigenous organic matter sources and reactivity in the North Atlantic  
 961 Ocean and a comparison to the Arctic and Pacific oceans. *Marine Chemistry*, 100(1-2), 66-79.  
 962 <https://doi.org/10.1016/j.marchem.2005.11.003>
- 963 Hertkorn, N., Benner, R., Frommberger, M., Schmitt-Kopplin, P., Witt, M., Kaiser, K., ... & Hedges, J. I. (2006).  
 964 Characterization of a major refractory component of marine dissolved organic matter. *Geochimica et*  
 965 *Cosmochimica Acta*, 70(12), 2990-3010. <https://doi.org/10.1016/j.gca.2006.03.021>
- 966 Hertkorn, N., Harir, M., Koch, B., Michalke, B., & Schmitt-Kopplin, P. (2013). High-field NMR spectroscopy  
 967 and FTICR mass spectrometry: powerful discovery tools for the molecular level characterization of marine  
 968 dissolved organic matter. *Biogeosciences*, 10, 1583-1624. <https://doi.org/10.5194/bg-10-1583-2013>
- 969 Hessen, D., & Tranvik, L. J. (Eds.). (2013). *Aquatic humic substances: ecology and biogeochemistry* (Vol. 133).  
 970 Springer Science & Business Media. <https://doi.org/10.1007/978-3-662-03736-2>
- 971 Hoge, F. E., Vodacek, A., & Blough, N. V. (1993). Inherent optical properties of the ocean: retrieval of the  
 972 absorption coefficient of chromophoric dissolved organic matter from fluorescence measurements. *Limnology*  
 973 *and Oceanography*, 38(7), 1394-1402. <https://doi.org/10.4319/lo.1993.38.7.1394>
- 974 Huber, S. A., Balz, A., Abert, M., & Pronk, W. (2011). Characterisation of aquatic humic and non-humic matter  
 975 with size-exclusion chromatography–organic carbon detection–organic nitrogen detection (LC-OCD-OND).  
 976 *Water research*, 45(2), 879-885. <https://doi.org/10.1016/j.watres.2010.09.023>
- 977 Huber, S. A., & Frimmel, F. H. (1994). Direct gel chromatographic characterization and quantification of marine  
 978 dissolved organic carbon using high-sensitivity DOC detection. *Environmental science & technology*, 28(6),  
 979 1194-1197. <https://doi.org/10.1021/es00055a035>
- 980 Hudson, N., Baker, A., & Reynolds, D. (2007). Fluorescence analysis of dissolved organic matter in natural,  
 981 waste and polluted waters—a review. *River research and applications*, 23(6), 631-649.  
 982 <https://doi.org/10.1002/rra.1005>
- 983 Huguet, A., Vacher, L., Relexans, S., Saubusse, S., Froidefond, J. M., & Parlanti, E. (2009). Properties of  
 984 fluorescent dissolved organic matter in the Gironde Estuary. *Organic Geochemistry*, 40(6), 706-719.  
 985 <https://doi.org/10.1016/j.orggeochem.2009.03.002>
- 986 Jiao, N., Herndl, G. J., Hansell, D. A., Benner, R., Kattner, G., Wilhelm, S. W., ... & Azam, F. (2010). Microbial  
 987 production of recalcitrant dissolved organic matter: long-term carbon storage in the global ocean. *Nature*  
 988 *Reviews Microbiology*, 8(8), 593-599. <https://doi.org/10.1038/nrmicro2386>
- 989 Kalbitz, K., Schwesig, D., Schmerwitz, J., Kaiser, K., Haumaier, L., Glaser, B., ... & Leinweber, P. (2003).  
 990 Changes in properties of soil-derived dissolved organic matter induced by biodegradation. *Soil Biology and*  
 991 *Biochemistry*, 35(8), 1129-1142. [https://doi.org/10.1016/S0038-0717\(03\)00165-2](https://doi.org/10.1016/S0038-0717(03)00165-2)
- 992  
 993 Kähler, P., & Koeve, W. (2001). Marine dissolved organic matter: can its C: N ratio explain carbon  
 994 overconsumption?. *Deep Sea Research Part I: Oceanographic Research Papers*, 48(1), 49-62.  
 995 [https://doi.org/10.1016/S0967-0637\(00\)00034-0](https://doi.org/10.1016/S0967-0637(00)00034-0)
- 996  
 997 Kieber, R. J., Hydro, L. H., & Seaton, P. J. (1997). Photooxidation of triglycerides and fatty acids in seawater:  
 998 Implication toward the formation of marine humic substances. *Limnology and Oceanography*, 42(6), 1454-1462.  
 999 <https://doi.org/10.4319/lo.1997.42.6.1454>
- 1000 Kikuchi, T., Fujii, M., Terao, K., Jiwei, R., Lee, Y. P., & Yoshimura, C. (2017). Correlations between  
 1001 aromaticity of dissolved organic matter and trace metal concentrations in natural and effluent waters: A case  
 1002 study in the Sagami River Basin, Japan. *Science of the Total Environment*, 576, 36-45.  
 1003 <https://doi.org/10.1016/j.scitotenv.2016.10.068>

- 1004 Kinsey, J. D., Corradino, G., Ziervogel, K., Schnetzer, A., & Osburn, C. L. (2018). Formation of chromophoric  
 1005 dissolved organic matter by bacterial degradation of phytoplankton-derived aggregates. *Frontiers in Marine*  
 1006 *Science*, 4, 430. <https://doi.org/10.3389/fmars.2017.00430>
- 1007 Koshlyakov, M. N., & Tarakanov, R. Y. (1999). Water masses of the Pacific Antarctic. *Oceanology*, 39(1), 1-11.  
 1008 <https://doi.org/10.1029/2007JC004549>
- 1009 Kowalenko, C. G., & McKercher, R. B. (1971). Phospholipid components extracted from Saskatchewan soils.  
 1010 *Canadian Journal of Soil Science*, 51(1), 19-22. <https://doi.org/10.4141/cjss71-003>
- 1011 Kujawinski, E. B. (2011). The impact of microbial metabolism on marine dissolved organic matter. *Annual*  
 1012 *review of marine science*, 3, 567-599. <https://doi.org/10.1146/annurev-marine-120308-081003>
- 1013 Kujawinski, E. B., Longnecker, K., Blough, N. V., Del Vecchio, R., Finlay, L., Kitner, J. B., & Giovannoni, S. J.  
 1014 (2009). Identification of possible source markers in marine dissolved organic matter using ultrahigh resolution  
 1015 mass spectrometry. *Geochimica et Cosmochimica Acta*, 73(15), 4384-4399.  
 1016 <https://doi.org/10.1016/j.gca.2009.04.033>
- 1017 Laglera, L. M., Battaglia, G., & van den Berg, C. M. (2007). Determination of humic substances in natural  
 1018 waters by cathodic stripping voltammetry of their complexes with iron. *Analytica chimica acta*, 599(1), 58-66.  
 1019 <https://doi.org/10.1016/j.aca.2007.07.059>
- 1020 Laglera, L. M., Sukekava, C., Slagter, H. A., Downes, J., Aparicio-Gonzalez, A., & Gerringa, L. J. (2019). First  
 1021 quantification of the controlling role of humic substances in the transport of iron across the surface of the Arctic  
 1022 Ocean. *Environmental science & technology*, 53(22), 13136-13145. <https://doi.org/10.1021/acs.est.9b04240>
- 1023 Laglera, L. M., & van den Berg, C. M. (2009). Evidence for geochemical control of iron by humic substances in  
 1024 seawater. *Limnology and Oceanography*, 54(2), 610-619. <https://doi.org/10.4319/lo.2009.54.2.0610>
- 1025 Lahajnar, N., Rixen, T., Gaye-Haake, B., Schäfer, P., & Ittekkot, V. (2005). Dissolved organic carbon (DOC)  
 1026 fluxes of deep-sea sediments from the Arabian Sea and NE Atlantic. *Deep Sea Research Part II: Topical Studies*  
 1027 *in Oceanography*, 52(14-15), 1947-1964. <https://doi.org/10.1016/j.dsr2.2005.05.006>
- 1028 Lara, R. J., Hubberten, U., & Kattner, G. (1993). Contribution of humic substances to the dissolved nitrogen pool  
 1029 in the Greenland Sea. *Marine chemistry*, 41(4), 327-336. [https://doi.org/10.1016/0304-4203\(93\)90264-O](https://doi.org/10.1016/0304-4203(93)90264-O)
- 1030 Lehmann, J., & Kleber, M. (2015). The contentious nature of soil organic matter. *Nature*, 528(7580), 60-68.  
 1031 <https://doi.org/10.1038/nature16069>
- 1032 Letscher, R. T., & Moore, J. K. (2015). Preferential remineralization of dissolved organic phosphorus and non-  
 1033 Redfield DOM dynamics in the global ocean: Impacts on marine productivity, nitrogen fixation, and carbon  
 1034 export. *Global Biogeochemical Cycles*, 29(3), 325-340. <https://doi.org/10.1002/2014GB004904>
- 1035 Lian, J., Zheng, X., Zhuo, X., Chen, Y. L., He, C., Zheng, Q., ... & Cai, R. (2021). Microbial transformation of  
 1036 distinct exogenous substrates into analogous composition of recalcitrant dissolved organic matter. *Environmental*  
 1037 *Microbiology*, 23(5), 2389-2403. <https://doi.org/10.1111/1462-2920.15426>
- 1039 Mackenzie, F. T. (1981). Global carbon cycle: Some minor sinks for CO<sub>2</sub>, in Flux of Organic Carbon by Rivers  
 1040 to the Oceans, edited by G. E. Likens, F. T. MacKenzie, J. E. Richey, J. R. Sedell, and K. K. Turekian, pp. 360-  
 1041 384, U.S. Department of Energy, Washington, D.C.
- 1042 Maillard, L. C. (1912). Condensation des acides aminés sur les sucres; formation de melanoidines par voie  
 1043 méthodique. *CR Acad Sci Paris*, 154, 66-8.
- 1044 Malcolm, R. L. (1990). The uniqueness of humic substances in each of soil, stream and marine environments.  
 1045 *Analytica Chimica Acta*, 232, 19-30. [https://doi.org/10.1016/S0003-2670\(00\)81222-2](https://doi.org/10.1016/S0003-2670(00)81222-2)



- 1046 Marques, J. S., Dittmar, T., Niggemann, J., Almeida, M. G., Gomez-Saez, G. V., & Rezende, C. E. (2017).  
 1047 Dissolved black carbon in the headwaters-to-ocean continuum of Paraiba Do Sul River, Brazil. *Frontiers in*  
 1048 *Earth Science*, 5, 11. <https://doi.org/10.3389/feart.2017.00011>
- 1049 McCartney, M. S. (1979). Subantarctic mode water. *Woods Hole Oceanographic Institution Contribution*, 3773,  
 1050 103-119.
- 1051 McKnight, D. M., Boyer, E. W., Westerhoff, P. K., Doran, P. T., Kulbe, T., & Andersen, D. T. (2001).  
 1052 Spectrofluorometric characterization of dissolved organic matter for indication of precursor organic material and  
 1053 aromaticity. *Limnology and Oceanography*, 46(1), 38-48. <https://doi.org/10.4319/lo.2001.46.1.0038>
- 1054 Medeiros, P. M., Seidel, M., Powers, L. C., Dittmar, T., Hansell, D. A., & Miller, W. L. (2015). Dissolved  
 1055 organic matter composition and photochemical transformations in the northern North Pacific Ocean.  
 1056 *Geophysical Research Letters*, 42(3), 863-870. <https://doi.org/10.1002/2014GL062663>
- 1057 Menzel, D. W., & Vaccaro, R. F. (1964). The measurement of dissolved organic and particulate carbon in  
 1058 seawater 1. *Limnology and Oceanography*, 9(1), 138-142. <https://doi.org/10.4319/lo.1964.9.1.0138>
- 1059 Miranda, M. L., Mustaffa, N. I. H., Robinson, T. B., Stolle, C., Ribas-Ribas, M., Wurl, O., ... & Blomquist, B.  
 1060 (2018). Influence of solar radiation on biogeochemical parameters and fluorescent dissolved organic matter  
 1061 (FDOM) in the sea surface microlayer of the southern coastal North Sea. *Elementa: Science of the*  
 1062 *Anthropocene*, 6. <https://doi.org/10.1525/elementa.278>
- 1063 Miranda, M. L., Osterholz, H., Giebel, H. A., Bruhnke, P., Dittmar, T., & Zielinski, O. (2020). Impact of UV  
 1064 radiation on DOM transformation on molecular level using FT-ICR-MS and PARAFAC. *Spectrochimica Acta*  
 1065 *Part A: Molecular and Biomolecular Spectroscopy*, 230, 118027. <https://doi.org/10.1016/j.saa.2020.118027>
- 1066 Mopper, K., Stubbins, A., Ritchie, J. D., Bialk, H. M., & Hatcher, P. G. (2007). Advanced instrumental  
 1067 approaches for characterization of marine dissolved organic matter: extraction techniques, mass spectrometry,  
 1068 and nuclear magnetic resonance spectroscopy. *Chemical Reviews*, 107(2), 419-442.  
 1069 <https://doi.org/10.1021/cr050359b>
- 1070 Nakane, M., Ajioka, T., & Yamashita, Y. (2017). Distribution and sources of dissolved black carbon in surface  
 1071 waters of the Chukchi Sea, Bering Sea, and the North Pacific Ocean. *Frontiers in earth science*, 5, 34.  
 1072 <https://doi.org/10.3389/feart.2017.00034>
- 1073 Ogawa, H., & Tanoue, E. (2003). Dissolved organic matter in oceanic waters. *Journal of Oceanography*, 59(2),  
 1074 129-147. <https://doi.org/10.1023/A:1025528919771>
- 1075 Ohno, T., Chorover, J., Omoike, A., & Hunt, J. (2007). Molecular weight and humification index as predictors of  
 1076 adsorption for plant-and manure-derived dissolved organic matter to goethite. *European Journal of Soil Science*,  
 1077 58(1), 125-132. <https://doi.org/10.1111/j.1365-2389.2006.00817.x>
- 1078 Opsahl, S., & Benner, R. (1997). Distribution and cycling of terrigenous dissolved organic matter in the ocean.  
 1079 *Nature*, 386(6624), 480-482. <https://doi.org/10.1038/386480a0>
- 1080 Osburn, C. L., Boyd, T. J., Montgomery, M. T., Bianchi, T. S., Coffin, R. B., & Paerl, H. W. (2016). Optical  
 1081 proxies for terrestrial dissolved organic matter in estuaries and coastal waters. *Frontiers in Marine Science*, 2,  
 1082 127. <https://doi.org/10.3389/fmars.2015.00127>
- 1083 Osburn, C. L., Kinsey, J. D., Bianchi, T. S., & Shields, M. R. (2019). Formation of planktonic chromophoric  
 1084 dissolved organic matter in the ocean. *Marine Chemistry*, 209, 1-13.  
 1085 <https://doi.org/10.1016/j.marchem.2018.11.010>
- 1086 Osterholz, H., Kilgour, D. P., Storey, D. S., Lavik, G., Ferdelman, T. G., Niggemann, J., & Dittmar, T. (2021).  
 1087 Accumulation of DOC in the South Pacific Subtropical Gyre from a molecular perspective. *Marine Chemistry*,  
 1088 231, 103955. <https://doi.org/10.1016/j.marchem.2021.103955>
- 1089 Para, J., Coble, P. G., Charrière, B., Tedetti, M., Fontana, C., & Sempere, R. (2010). Fluorescence and  
 1090 absorption properties of chromophoric dissolved organic matter (CDOM) in coastal surface waters of the

- 1091 northwestern Mediterranean Sea, influence of the Rhône River. *Biogeosciences*, 7(12), 4083-4103.  
1092 <https://doi.org/10.5194/bg-7-4083-2010>
- 1093 Paerl, R. W., Claudio, I. M., Shields, M. R., Bianchi, T. S., & Osburn, C. L. (2020). Dityrosine formation via  
1094 reactive oxygen consumption yields increasingly recalcitrant humic-like fluorescent organic matter in the ocean.  
1095 *Limnology and Oceanography Letters*, 5(5), 337-345. <https://doi.org/10.1002/lol2.10154>
- 1096 Parlanti, E., Wörz, K., Geoffroy, L., & Lamotte, M. (2000). Dissolved organic matter fluorescence spectroscopy  
1097 as a tool to estimate biological activity in a coastal zone submitted to anthropogenic inputs. *Organic*  
1098 *geochemistry*, 31(12), 1765-1781. [https://doi.org/10.1016/S0146-6380\(00\)00124-8](https://doi.org/10.1016/S0146-6380(00)00124-8)
- 1099 Peters, B. D., Jenkins, W. J., Swift, J. H., German, C. R., Moffett, J. W., Cutter, G. A., ... & Casciotti, K. L.  
1100 (2018). Water mass analysis of the 2013 US GEOTRACES eastern Pacific zonal transect (GP16). *Marine*  
1101 *Chemistry*, 201, 6-19. <https://doi.org/10.1016/j.marchem.2017.09.007>
- 1102 Polimene, L., Rivkin, R. B., Luo, Y. W., Kwon, E. Y., Gehlen, M., Pena, M. A., ... & Jiao, N. (2018). Modelling  
1103 marine DOC degradation time scales. *National Science Review*, 5(4), 468-474.  
1104 <https://doi.org/10.1093/nsr/nwy066>
- 1105 Poulin, B. A., Ryan, J. N., & Aiken, G. R. (2014). Effects of iron on optical properties of dissolved organic  
1106 matter. *Environmental Science & Technology*, 48(17), 10,098–10,106. <https://doi.org/10.1021/es502670r>
- 1107 Powell, R. T., & Donat, J. R. (2001). Organic complexation and speciation of iron in the South and Equatorial  
1108 Atlantic. *Deep Sea Research Part II: Topical Studies in Oceanography*, 48(13), 2877-2893.  
1109 [https://doi.org/10.1016/S0967-0645\(01\)00022-4](https://doi.org/10.1016/S0967-0645(01)00022-4)
- 1110 Repeta, D. J., Quan, T. M., Aluwihare, L. I., & Accardi, A. (2002). Chemical characterization of high molecular  
1111 weight dissolved organic matter in fresh and marine waters. *Geochimica et Cosmochimica Acta*, 66(6), 955-962.  
1112 [https://doi.org/10.1016/S0016-7037\(01\)00830-4](https://doi.org/10.1016/S0016-7037(01)00830-4)
- 1113 Riso, R., Mastin, M., Aschehoug, A., Davy, R., Devesa, J., Laës-Huon, A, Waeles, M. & Dulaquais, G. (2021).  
1114 Distribution, speciation and composition of humic substances in a macro-tidal temperate estuary. *Estuarine,*  
1115 *Coastal and Shelf Science*, 107360. <https://doi.org/10.1016/j.ecss.2021.107360>
- 1116 Rue, E. L., & Bruland, K. W. (1995). Complexation of iron (III) by natural organic ligands in the Central North  
1117 Pacific as determined by a new competitive ligand equilibration/adsorptive cathodic stripping voltammetric  
1118 method. *Marine chemistry*, 50(1-4), 117-138. [https://doi.org/10.1016/0304-4203\(95\)00031-L](https://doi.org/10.1016/0304-4203(95)00031-L)
- 1119 Rue, E. L., & Bruland, K. W. (1997). The role of organic complexation on ambient iron chemistry in the  
1120 equatorial Pacific Ocean and the response of a mesoscale iron addition experiment. *Limnology and*  
1121 *oceanography*, 42(5), 901-910. <https://doi.org/10.4319/lo.1997.42.5.0901>
- 1122 Segnini, A., Posadas, A., Quiroz, R., Milori, D. M. B. P., Saab, S. C., Neto, L. M., & Vaz, C. M. P. (2010).  
1123 Spectroscopic assessment of soil organic matter in wetlands from the high Andes. *Soil Science Society of*  
1124 *America Journal*, 74(6), 2246-2253. <https://doi.org/10.2136/sssaj2009.0445>
- 1125 Shen, Y., & Benner, R. (2018). Mixing it up in the ocean carbon cycle and the removal of refractory dissolved  
1126 organic carbon. *Scientific reports*, 8(1), 1-9. <https://doi.org/10.1038/s41598-018-20857-5>
- 1127 Shen, Y., & Benner, R. (2020). Molecular properties are a primary control on the microbial utilization of  
1128 dissolved organic matter in the ocean. *Limnology and Oceanography*, 65(5), 1061-1071.  
1129 <https://doi.org/10.1002/lno.11369>
- 1130 Silva, N., Rojas, N., & Fedele, A. (2009). Water masses in the Humboldt Current System: Properties,  
1131 distribution, and the nitrate deficit as a chemical water mass tracer for Equatorial Subsurface Water off Chile.  
1132 *Deep Sea Research Part II: Topical Studies in Oceanography*, 56(16), 1004-1020.  
1133 <https://doi.org/10.1016/j.dsr2.2008.12.013>

- 1134 Slagter, H. A., Laglera, L. M., Sukekava, C., & Gerringa, L. J. (2019). Fe-binding organic ligands in the humic-  
 1135 rich TransPolar Drift in the surface Arctic Ocean using multiple voltammetric methods. *Journal of Geophysical*  
 1136 *Research: Oceans*, 124(3), 1491-1508. <https://doi.org/10.1029/2018JC014576>
- 1137 Sohrin, R., & Sempéré, R. (2005). Seasonal variation in total organic carbon in the northeast Atlantic in 2000–  
 1138 2001. *Journal of Geophysical Research: Oceans*, 110(C10). <https://doi.org/10.1029/2004JC002731>
- 1139 Sprintall, J., & Tomczak, M. (1993). On the formation of Central Water and thermocline ventilation in the  
 1140 southern hemisphere. *Deep Sea Research Part I: Oceanographic Research Papers*, 40(4), 827-848.  
 1141 [https://doi.org/10.1016/0967-0637\(93\)90074-D](https://doi.org/10.1016/0967-0637(93)90074-D)
- 1142 Stedmon, C. A., Markager, S., & Bro, R. (2003). Tracing dissolved organic matter in aquatic environments using  
 1143 a new approach to fluorescence spectroscopy. *Marine chemistry*, 82(3-4), 239-254.  
 1144 [https://doi.org/10.1016/S0304-4203\(03\)00072-0](https://doi.org/10.1016/S0304-4203(03)00072-0)
- 1145 Stott, D. E., & Martin, J. P. (1990). Synthesis and degradation of natural and synthetic humic material in soils.  
 1146 *Humic substances in soil and crop sciences: Selected readings*, 37-63.  
 1147 <https://doi.org/10.2136/1990.humicsubstances.c3>
- 1148 Sukekava, C., Downes, J., Slagter, H. A., Gerringa, L. J., & Laglera, L. M. (2018). Determination of the  
 1149 contribution of humic substances to iron complexation in seawater by catalytic cathodic stripping voltammetry.  
 1150 *Talanta*, 189, 359-364. <https://doi.org/10.1016/j.talanta.2018.07.021>
- 1151 Swan, C. M., Siegel, D. A., Nelson, N. B., Carlson, C. A., & Nasir, E. (2009). Biogeochemical and hydrographic  
 1152 controls on chromophoric dissolved organic matter distribution in the Pacific Ocean. *Deep Sea Research Part I:*  
 1153 *Oceanographic Research Papers*, 56(12), 2175-2192. <https://doi.org/10.1016/j.dsr.2009.09.002>
- 1154 Tedetti, M., Cuet, P., Guigue, C., & Goutx, M. (2011). Characterization of dissolved organic matter in a coral  
 1155 reef ecosystem subjected to anthropogenic pressures (La Réunion Island, Indian Ocean) using multi-dimensional  
 1156 fluorescence spectroscopy. *Science of the total environment*, 409(11), 2198-2210.  
 1157 <https://doi.org/10.1016/j.scitotenv.2011.01.058>
- 1158 Tomczak, M., & Godfrey, J. S. (2003). *Regional oceanography: an introduction*. Daya books.  
 1159 <https://doi.org/10.1016/C2009-0-14825-0>
- 1160 van den Berg, C. M. (1995). Evidence for organic complexation of iron in seawater. *Marine Chemistry*, 50(1-4),  
 1161 139-157. [https://doi.org/10.1016/0304-4203\(95\)00032-M](https://doi.org/10.1016/0304-4203(95)00032-M)
- 1162 Villa-Alfageme, M., Chamizo, E., Kenna, T. C., López-Lora, M., Casacuberta, N., Chang, C., ... & Christl, M.  
 1163 (2019). Distribution of <sup>236</sup>U in the US GEOTRACES Eastern Pacific Zonal Transect and its use as a water mass  
 1164 tracer. *Chemical Geology*, 517, 44-57. <https://doi.org/10.1016/j.chemgeo.2019.04.003>
- 1165 Wagener, T., Metzl, N., Caffin, M., Fin, J., Helias Nunige, S., Lefevre, D., ... & Moutin, T. (2018). Carbonate  
 1166 system distribution, anthropogenic carbon and acidification in the western tropical South Pacific (OUTPACE  
 1167 2015 transect). *Biogeosciences*, 15(16), 5221-5236. <https://doi.org/10.5194/bg-15-5221-2018>
- 1168 Wagner, S., Jaffé, R., & Stubbins, A. (2018). Dissolved black carbon in aquatic ecosystems. *Limnology and*  
 1169 *Oceanography Letters*, 3(3), 168-185. <https://doi.org/10.1002/lol2.10076>
- 1170 Weiss, R. F. (1970). The solubility of nitrogen, oxygen and argon in water and seawater. In *Deep Sea Research*  
 1171 *and Oceanographic Abstracts* (Vol. 17, No. 4, pp. 721-735). Elsevier. [https://doi.org/10.1016/0011-7471\(70\)90037-9](https://doi.org/10.1016/0011-7471(70)90037-9)
- 1173 Whitby, H., Bressac, M., Sarthou, G., Ellwood, M. J., Guieu, C., & Boyd, P. W. (2020a). Contribution of  
 1174 electroactive humic substances to the iron-binding ligands released during microbial remineralization of sinking  
 1175 particles. *Geophysical Research Letters*, 47(7). <https://doi.org/10.1029/2019GL086685>
- 1176 Whitby, H., Planquette, H., Cassar, N., Bucciarelli, E., Osburn, C. L., Janssen, D. J., ... & Sarthou, G. (2020b). A  
 1177 call for refining the role of humic-like substances in the oceanic iron cycle. *Scientific reports*, 10(1), 1-12.  
 1178 <https://doi.org/10.1038/s41598-020-62266-7>

- 1179 Wyrski, K. (1967). Equatorial Pacific Ocean I. *Int. J. Oceanol. & Limnol. Vol, 1*(2), 117-147.
- 1180 Whitby, H., & van den Berg, C. M. (2015). Evidence for copper-binding humic substances in seawater. *Marine*  
1181 *Chemistry, 173*, 282-290. <https://doi.org/10.1016/j.marchem.2014.09.011>
- 1182 Wu, J., & Luther III, G. W. (1995). Complexation of Fe (III) by natural organic ligands in the Northwest Atlantic  
1183 Ocean by a competitive ligand equilibration method and a kinetic approach. *Marine Chemistry, 50*(1-4), 159-  
1184 177. [https://doi.org/10.1016/0304-4203\(95\)00033-N](https://doi.org/10.1016/0304-4203(95)00033-N)
- 1185 Wünsch, U. J., Bro, R., Stedmon, C. A., Wenig, P., & Murphy, K. R. (2019). Emerging patterns in the global  
1186 distribution of dissolved organic matter fluorescence. *Analytical Methods, 11*(7), 888-893.  
1187 <https://doi.org/10.1039/C8AY02422G>
- 1188 Yamashita, Y., Cory, R. M., Nishioka, J., Kuma, K., Tanoue, E., & Jaffé, R. (2010). Fluorescence characteristics  
1189 of dissolved organic matter in the deep waters of the Okhotsk Sea and the northwestern North Pacific Ocean.  
1190 *Deep Sea Research Part II: Topical Studies in Oceanography, 57*(16), 1478-1485.  
1191 <https://doi.org/10.1016/j.dsr2.2010.02.016>
- 1192 Yamashita, Y., & Tanoue, E. (2004). In situ production of chromophoric dissolved organic matter in coastal  
1193 environments. *Geophysical Research Letters, 31*(14). <https://doi.org/10.1029/2004GL019734>
- 1194 Yamashita, Y., & Jaffé, R. (2008). Characterizing the interactions between trace metals and dissolved organic  
1195 matter using excitation-emission matrix and parallel factor analysis. *Environmental Science &*  
1196 *Technology, 42*(19), 7374–7379. <https://doi.org/10.1021/es801357h>
- 1197 Yamashita, Y., & Tanoue, E. (2008). Production of bio-refractory fluorescent dissolved organic matter in the  
1198 ocean interior. *Nature Geoscience, 1*(9), 579-582. <https://doi.org/10.1038/ngeo279>
- 1199 Yamashita, Y., & Tanoue, E. (2009). Basin scale distribution of chromophoric dissolved organic matter in the  
1200 Pacific Ocean. *Limnology and Oceanography, 54*(2), 598-609. <https://doi.org/10.4319/lo.2009.54.2.0598>
- 1201 Zark, M., Christoffers, J., & Dittmar, T. (2017). Molecular properties of deep-sea dissolved organic matter are  
1202 predictable by the central limit theorem: evidence from tandem FT-ICR-MS. *Marine Chemistry, 191*, 9-15.  
1203 <https://doi.org/10.1016/j.marchem.2017.02.005>
- 1204 Zhao, S., Xue, S., Zhang, J., Zhang, Z., & Sun, J. (2020). Dissolved organic matter-mediated photodegradation  
1205 of anthracene and pyrene in water. *Scientific Reports, 10*(1), 1-9. <https://doi.org/10.1038/s41598-020-60326-6>  
1206
- 1207 Zheng, Q., Chen, Q., Cai, R., He, C., Guo, W., Wang, Y., ... & Jiao, N. (2019). Molecular characteristics of  
1208 microbially mediated transformations of Synechococcus-derived dissolved organic matter as revealed by  
1209 incubation experiments. *Environmental microbiology, 21*(7), 2533-2543. [https://doi.org/10.1111/1462-  
1210 2920.14646](https://doi.org/10.1111/1462-2920.14646)
- 1211 Zigah, P. K., McNichol, A. P., Xu, L., Johnson, C., Santinelli, C., Karl, D. M., & Repeta, D. J. (2017).  
1212 Allochthonous sources and dynamic cycling of ocean dissolved organic carbon revealed by carbon isotopes.  
1213 *Geophysical Research Letters, 44*(5), 2407-2415. <https://doi.org/10.1002/2016GL071348>
- 1214 Ziolkowski, L. A., & Druffel, E. R. (2010). Aged black carbon identified in marine dissolved organic carbon.  
1215 *Geophysical Research Letters, 37*(16). <https://doi.org/10.1029/2010GL043963>
- 1216 Zsolnay, Á. (2003). Dissolved organic matter: artefacts, definitions, and functions. *Geoderma, 113*(3-4), 187-  
1217 209. [https://doi.org/10.1016/S0016-7061\(02\)00361-0](https://doi.org/10.1016/S0016-7061(02)00361-0)
- 1218 Zsolnay, A., Baigar, E., Jimenez, M., Steinweg, B., & Saccomandi, F. (1999). Differentiating with fluorescence  
1219 spectroscopy the sources of dissolved organic matter in soils subjected to drying. *Chemosphere, 38*(1), 45-50.  
1220 [https://doi.org/10.1016/S0045-6535\(98\)00166-0](https://doi.org/10.1016/S0045-6535(98)00166-0)



1221 **Supplementary material**

1222

1223 **Table S1.** Limits of detection (LOD) for the different detectors coupled to SEC in a seawater matrix  
 1224 (Bay of Brest, S = 35 psu). Injection volumes were 2 mL. LOD were calculated according to the  
 1225 IUPAC recommendation (1978):  $LOD = 3 \times SE$  where « SE » is the mean standard error (or standard  
 1226 error) of the blanks over 10 consecutive measurements of a coastal water of the Bay of Brest,  
 1227 previously irradiated (3h) with UV light (Dulaquais et al., 2018b). The expected contents in each  
 1228 fraction operationally defined by SEC are those proposed by Huber et al. (2011) and in this study.

Organic carbon (μMC)						
Fraction	DOC	BP	HS	BB	LMW acids	LMW neutrals
Expected content	Huber et al. (2011)	Proteinic matter Polysaccharides	Humic matter including	HS-like material of LMW	Anions at the pH of the buffer (~ 7)	Hydrophilic/amphiphilic compounds of low ion density
	This study		Fulvic and humic acids	Degradation by-products of BP		
LOD	2.3	0.4	0.2	0.1	1.0	3.0
Organic nitrogen (μMN)			Aromatic carbon (%)			
Fraction	BP	HS	BP	HS		
LOD	0.2	0.2	0.6	0.1		

1229

1230

1231

1232

1233

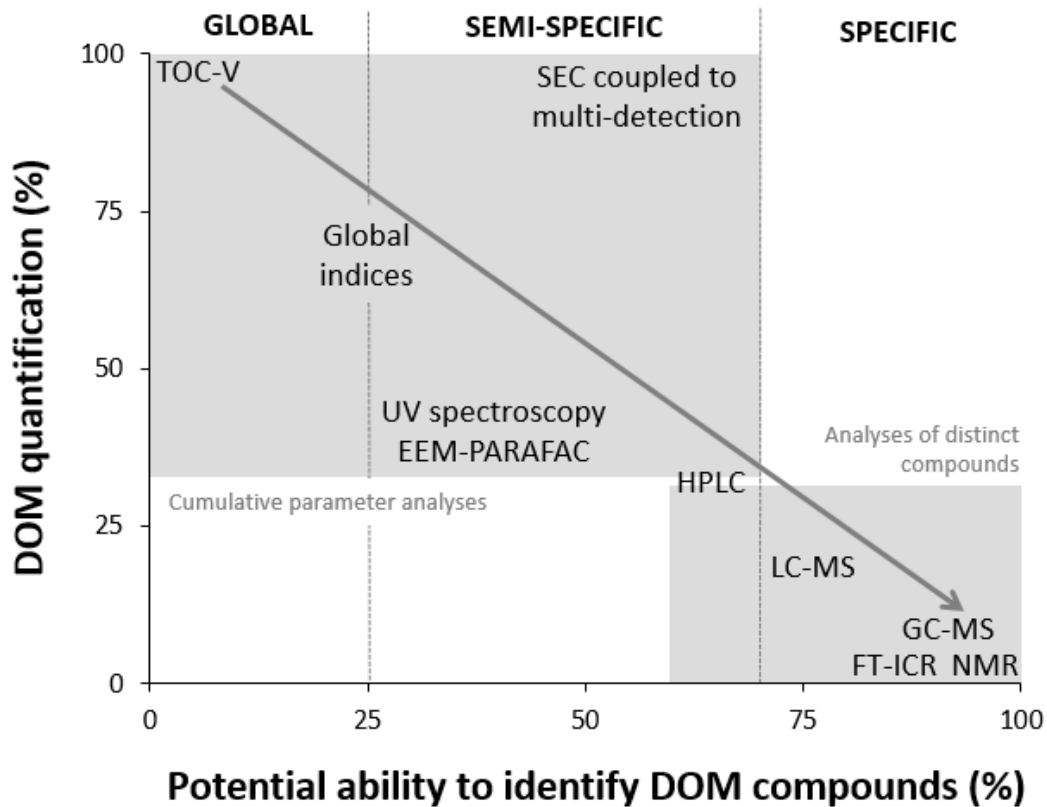
1234 **Table S2.** Analyses performed on DOM for each different cruise presented in this study. TOC-V  
 1235 analyses during CLIVAR (\*) were carried out by Swan et al. (2009).

Cruise – Station – Coordinates	Analytical method			
	SEC	TOC-V	Fluorescence	CSV (eHs)
<b>TONGA – St. 8</b> – 20° 24.431'S, 166° 35.675'W	✓	✓	✓	✓
<b>US-GP15 – St. 39</b> – 19° 59.99'S, 152° 00.01'W	✓			
<b>CLIVAR P16 – St.9</b> – 20°S; 150°W		✓*		

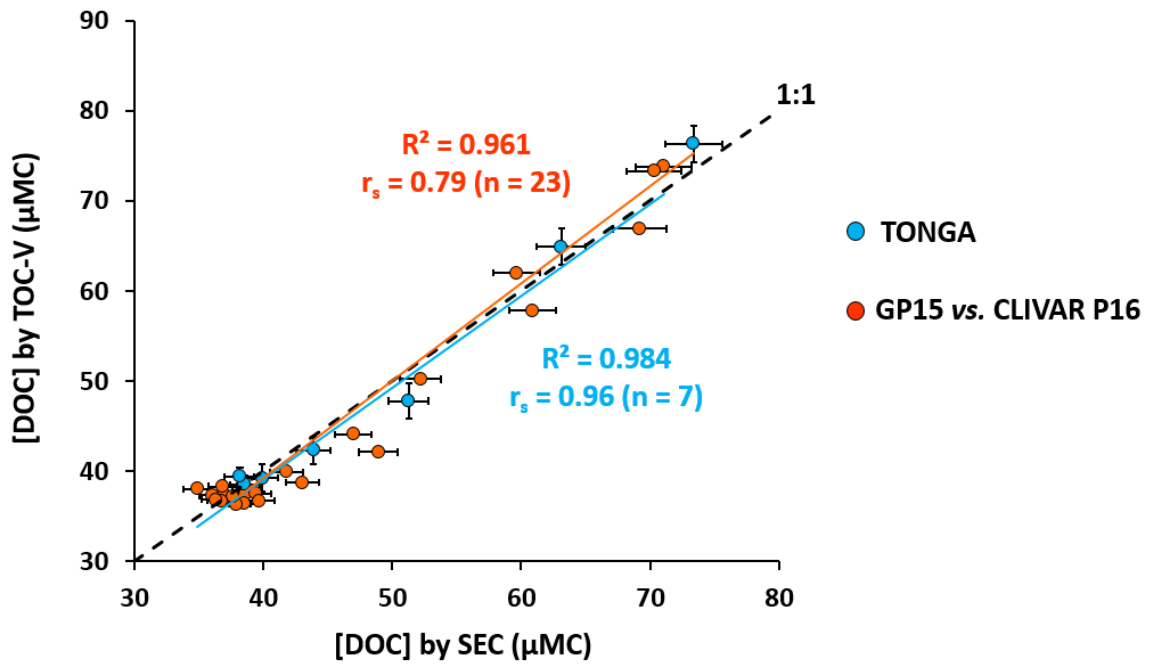
1236

1237

1238

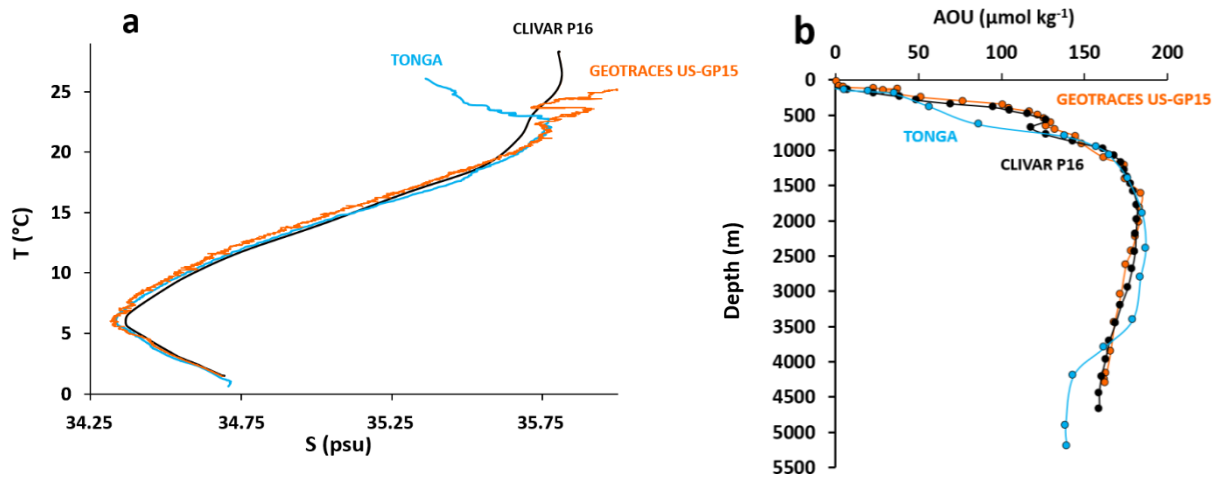


1239 **Figure S1.** Analytical window of the different approaches applied to DOM analysis. TOC = Total  
 1240 Organic Carbon; SEC: Size Exclusion Chromatography; EEM-PARAFAC: Excitation Emission  
 1241 fluorescence Matrice-Parallel Factor Analysis; HPLC: High Performance Liquid Chromatography;  
 1242 LC-MS: Liquid Chromatography-Mass Spectrometry; GC-MS: Gas Chromatography-Mass  
 1243 Spectrometry; FT-ICR: Fourier Transform Ion Cyclotron Resonance; NMR: Nuclear Magnetic  
 1244 Resonance. Figure based on [http://doc-labor.de/?page\\_id=13](http://doc-labor.de/?page_id=13).

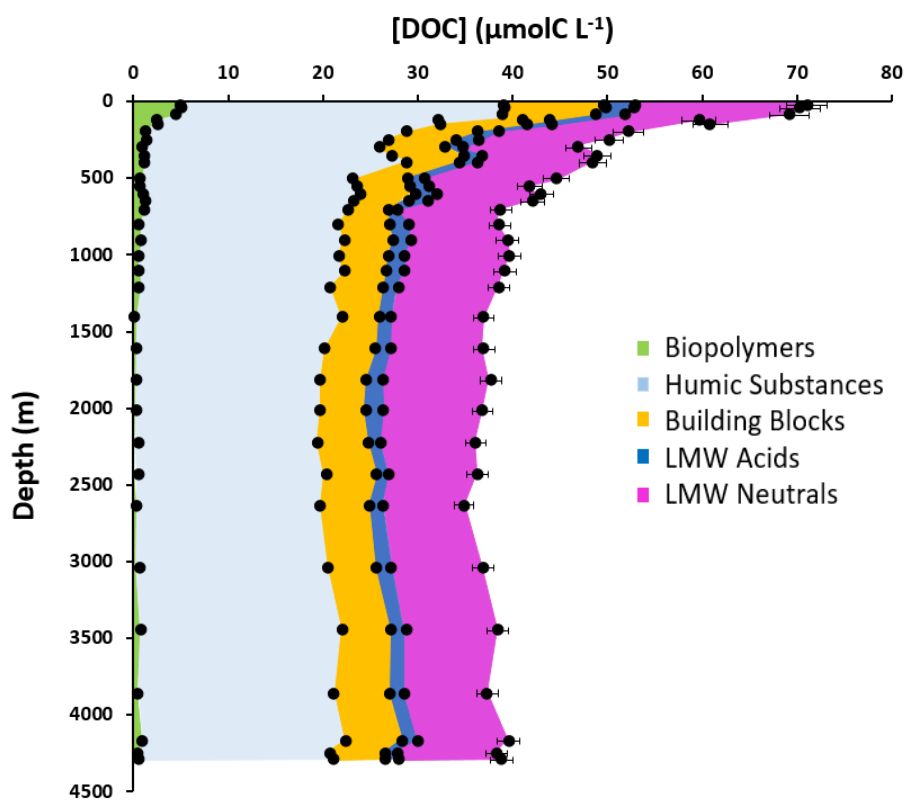


1245  
 1246  
 1247  
 1248  
 1249  
 1250

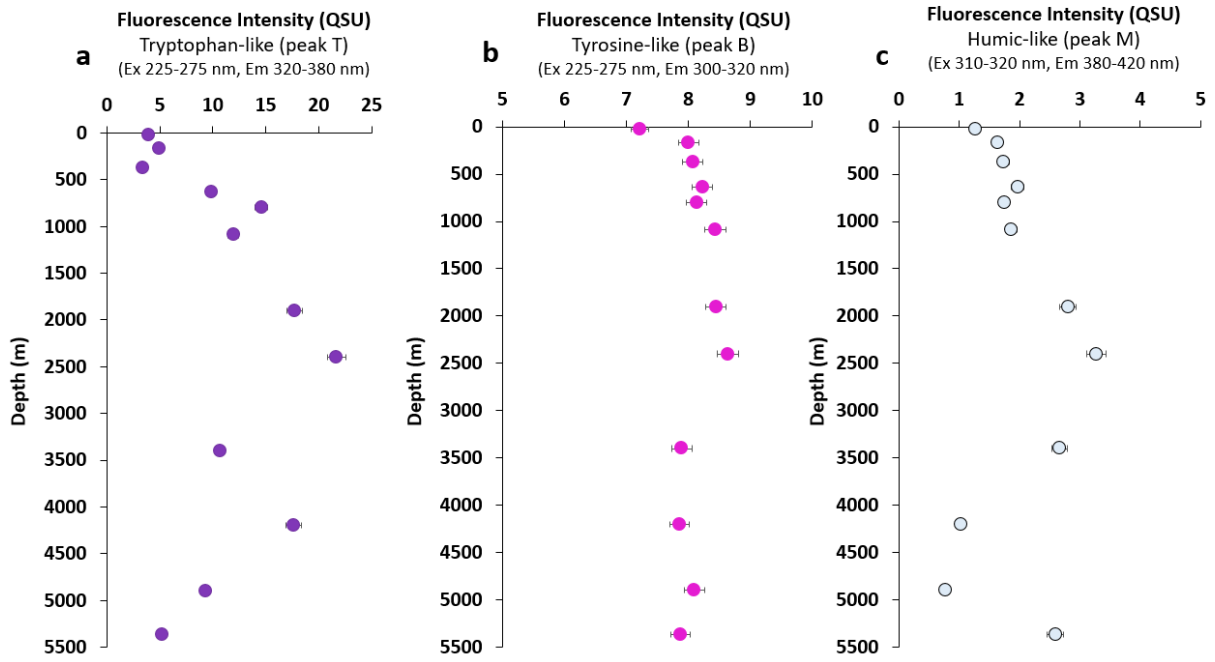
**Figure S2.** Comparisons between the datasets from GP15 St. 39 ( $19^\circ 59.99'S$ ,  $152^\circ 00.01'W$ ) by SEC and historical data from CLIVAR P16 St. 9 ( $20^\circ S$ ;  $150^\circ W$ ) by TOC-V, as well as the two TONGA datasets (SEC and TOC-V) at St. 8 ( $20^\circ 24.431'S$ ,  $166^\circ 35.675'W$ ). Spearman coefficient  $r_s$  close to 1 in both cases indicates the strong correlation between DOC concentrations determined by TOC-V and SEC.



1251 **Figure S3.** (a) Intercomparison of the temperature/salinity AOU diagram between TONGA St. 8 (20°  
 1252 24.431'S, 166° 35.675'W), GEOTRACES US-GP15 St. 39 (19° 59.99'S, 152° 00.01'W) and  
 1253 CLIVAR P16 St. 9 (20°S; 150°W). (b) Intercomparison between vertical profiles of apparent oxygen  
 1254 utilization (AOU) for TONGA, GEOTRACES and CLIVAR P16 (same stations).



1255 **Figure S4.** Vertical profiles of the DOC concentrations ( $\mu\text{MC}$ ) in the five operational fractions  
 1256 defined by SEC, along the water column at  $19^\circ 59.99'S$ ,  $152^\circ 00.01'W$  during the GEOTRACES US-  
 1257 GP15 expedition. Non-visible error bars are covered by the symbols.



1259

1260

1261

1262

**Figure S5.** Vertical profiles of (a) tryptophan-like fluorescence intensity (T); (b) tyrosine-like fluorescence intensity (B); (c) marine humic-like fluorescence intensity (M); according to the nomenclature defined by Coble (1996).